Master in Chemical Engineering

Shaping, characterization, and measurement of adsorption properties of ZIF-8 and MIL-53(Al) adsorbents

Master's Dissertation

by

Ana Jorge Meireles Pereira

Developed for the dissertation course unit

at

LSRE – Laboratory of Separation and Reaction Engineering

ASSOCIATE LABORATORY
LABORATORY OF SEPARATION AND REACTION ENGINEERING
LABORATORY OF CATALYSIS AND MATERIALS

Supervisor: **Doctor Alexandre Ferreira**
Co-supervisor: **Eng. Maria João Regufe**
Co-supervisor: **Doctor Ana Mafalda Ribeiro**
Co-supervisor: **Professor Alírio Egídio Rodrigues**

U.PORTO
FEUP FACULDADE DE ENGENHARIA
UNIVERSIDADE DO PORTO

Departamento de Engenharia Química

July 2019

Agradecimentos / Acknowledgments

Gostaria de agradecer aos meus orientadores: Doutor Alexandre Ferreira, Doutora Ana Mafalda Ribeiro e Eng. Maria João Regufe pelo tempo despendido e por o apoio durante a realização deste trabalho. Queria deixar ainda um agradecimento especial à Eng. Maria João Regufe por aturar todas as minhas perguntas, até aos fim-de-semana e feriados. *FOSTE INCANSÁVEL, OBRIGADA!*

Deixo também um agradecimento ao Professor Alírio Egídio Rodrigues por disponibilizar o seu laboratório e instalações para a realização deste trabalho.

A vocês colegas de laboratório queria deixar um "obrigada" pelo companheirismo e por todos os bolos e bolachas que animam uma pessoa.

Queria ainda a agradecer aos meus amigos e família. Aos de Aveiro que me acompanham desde sempre e aos do Porto que apesar de recentes foram muito importantes durante o meu percurso académico.

E por último, mas ainda mais importantes aos meus pais, pelo esforço que fizeram durante estes 5 anos e pelo apoio incondicional neste percurso cheio de altos e baixos e ao meu CR3 que é o meu pilar, o meu suporte e o meu génio. CR3, sem ti nada disto era igual!

This work was financially supported: by Project NORTE-01-0145-FEDER-029384 funded by FEDER funds through NORTE 2020 - Programa Operacional Regional do NORTE – and by national funds (PIDDAC) through FCT/MCTES and by Associate Laboratory LSRE-LCM - UID/EQU/50020/2019 - funded by national funds through FCT/MCTES (PIDDAC).

Resumo

A separação/purificação e armazenamento de gases são processos cruciais na indústria química. Desta forma, as técnicas de adsorção são uma das ferramentas usadas neste campo. No entanto, de modo a obter um bom desempenho com estas técnicas, devem ser utilizados adsorventes com boa transferência de massa e calor, baixa queda de pressão e com grande estabilidade mecânica. Uma vez que o adsorvente é produzido na forma de pó, é essencial fazer o seu *shaping* de forma a obter as características mencionadas anteriormente. Tendo isto em conta, foram produzidos *pellets* e monólitos usando diferentes técnicas *shaping*, nomeadamente a extrusão e a impressão 3D. Para além disto, diferentes ligantes foram testados. Os adsorventes utilizados foram os pós de ZIF-8 e de MIL-53(Al) e os ligantes testados foram a alumina, a CMC, a *kaolin* e o PE. Os materiais preparados foram: *pellets* com ZIF-8 e 5, 10 e 15 %(m/m) de alumina (ZIF-8-PA5, ZIF-8-PA10 e ZIF-8-PA15), *pellets* com ZIF-8 e 5 e 10 %(m/m) de CMC (ZIF-8-PC5 e ZIF-8-PC10), *pellets* de MIL-53(Al) com 5, 10 e 15 %(m/m) de alumina (MIL-53(Al)-PA5, MIL-53(Al)-PA10 e MIL-53(Al)-PA15), monólitos com ZIF-8 e com 5 e 10 %(m/m) de CMC (ZIF-8-MC5 e ZIF-8-MC10) e um monólito de MIL-53(Al) com 5 %(m/m) de *kaolin* e com 5 %(m/m) de PE.

Antes de empregar a impressão 3D para produzir monólitos, a pasta contendo o adsorvente e os ligantes foi caracterizada reologicamente através de testes rotacionais e oscilatórios.

Após a preparação destes materiais, caracterização química e morfológica (SEM/EDS, isotérmicas de adsorção de N_2 a 77 K, isotérmicas de adsorção de CO_2 a 273 K, porosimetria de mercúrio e XRD) foi realizada para perceber o efeito do *shaping* nos adsorventes. Desta forma, o efeito da quantidade de ligante e do tipo de ligante foi estudado com o propósito de perceber qual é a quantidade ideal de ligante e qual o tipo de ligante que deve ser utilizado para garantir que o material produzido tem as características referidas anteriormente e que o ligante não afeta de forma significativa as propriedades de adsorção das estruturas que sofreram *shaping*.

Além das caracterizações mencionadas, foram realizados testes de resistência mecânica ao esmagamento dos *pellets* de alumina para compreender o efeito da técnica de *shaping* e da quantidade de ligante utilizado na estabilidade mecânica dos adsorventes preparados.

Finalmente, neste trabalho, as isotérmicas de equilíbrio de adsorção para CH_4 e N_2 foram determinadas a 303 K para valores de pressão até 4 bar. O modelo de adsorção de Langmuir foi utilizado para ajustar os resultados experimentais. Este estudo permitiu entender o efeito do *shaping* nas capacidades de adsorção do material e qual material possui as melhores propriedades para ser utilizado na separação de CH_4/N_2.

Palavras Chave: adsorção; separação N_2/CH_4; ZIF-8; MIL-53(Al); *shaping*; *pellets*; monólitos; caracterização.

Abstract

The separation, purification, and storage of gases are crucial processes of the chemical industry. In this way, adsorption techniques are one of the tools used in this field. However, to obtain good results with these techniques, adsorbents with high mass and heat transference, low-pressure drop and with high mechanical stability have to be used. Since adsorbents are produced in the powder form, it is essential to shape it to obtain the features previously mentioned. Taking this into account, pellets and monoliths were produced using different shaping techniques, namely extrusion and 3D printing. Moreover, different binder materials were tested. The primary adsorbents employed were ZIF-8 and MIL-53(Al) powders, and the tested binders were alumina, CMC, kaolin, and PE. The final prepared materials are: pellets with ZIF-8 and 5, 10 and 15 %wt. of alumina (ZIF-8-PA5, ZIF-8-PA10 and ZIF-8-PA15), pellets with ZIF-8 and 5 and 10 %wt. of CMC (ZIF-8-PC5 and ZIF-8-PC10), pellets of MIL-53(Al) with 5, 10 and 15 %wt. of alumina (MIL-53(Al)-PA5, MIL-53(Al)-PA10 and MIL-53(Al)-PA15), monoliths with ZIF-8 and 5 and 10 %wt. of CMC (ZIF-8-MC5 and ZIF-8-MC10) and a monolith with MIL-53(Al) and 5 %wt. of kaolin and 5 %wt. of PE (MIL-53(Al)-M).

Before using the 3D technique to produce monoliths, the ink containing the adsorbent and the binders was characterized through rotational and oscillatory rheological tests.

After the preparation of these materials, chemical and morphological characterization (SEM/EDS, N_2 adsorption equilibrium isotherms at 77 K, CO_2 adsorption equilibrium isotherms at 273 K, mercury porosimetry and XRD) was performed to comprehend the effect of the shaping in the adsorbent materials. In this way, the effect of the quantity of binder and the type of binder was studied, with the purpose of understanding which is the ideal quantity of binder and the type of binder that should be utilized. This study will allow the production of materials that have the features referred previously and to find out if the binder affects in a significant way the adsorption properties of the shaped structures.

Besides the characterization tests previously mentioned, radial crushing strength tests were performed on the shaped materials to comprehend the effect of the shaping technique and the amount of binder used in the mechanical stability of the shaped adsorbents.

Finally, the adsorption equilibrium isotherms for CH_4 and N_2 were determined at 303 K for pressure values up to 4 bar. Langmuir adsorption model was used to fit the experimental results. This study allows to understand the effect of shaping in the adsorption capacities of the material and which material has the best properties to be used in CH_4/N_2 separation.

Keywords: adsorption; N_2/CH_4 separation; ZIF-8; MIL-53(Al); shaping; pellets; monoliths, characterization.

Declaration

Declara, sob compromisso de honra, que este trabalho é original e que todas as contribuições não originais foram devidamente referenciadas com identificação da fonte.

Porto, 1 de julho de 2019

Ana Jorge Meireles Pereira

Table of contents

List of Figures

List of Tables

Notação e Glossário

b	adsorption equilibrium constant of component i	bar^{-1}
k	transition time	s
k_1	transition time	s
m	viscosity exponent	
m_1	viscosity exponent	
M	adsorbate molecular mass	$kg \cdot mol^{-1}$
m_s	mass of the solid adsorbent	kg
P	pressure	bar
q	quantity adsorbed	$mol \cdot kg^{-1}$
q_i	quantity adsorbed of the component i	$mol \cdot kg^{-1}$
q_j	quantity adsorbed of the component j	$mol \cdot kg^{-1}$
q_m	maximum adsorption capacity	$mol \cdot kg^{-1}$
V_c	volume of the basket	m^3
V_s	volume of the solid adsorbent	m^3
x_i	molar fraction of the component i	
x_j	molar fraction of the component j	

Letras gregas

$\alpha_{i,j}$	the selectivity between the component i and j	
Δm	difference between the measured weight and the weight when there is no gas in the cell	kg
$\dot{\gamma}$	shear rate	s^{-1}
ρ_G	density of the gas phase	$kg \cdot m^{-3}$
ρ_{ads}	density of the adsorbed phase	$kg \cdot m^{-3}$
η	viscosity	Pa·s
η_0	zero-shear viscosity	Pa·s
η_∞	infinite-shear viscosity	Pa·s

List of Acronyms

$AlPO_4$	Aluminium Phosphate
CMC	Carboxymethylcellulose
DI	Deionized water
DIW	Direct Ink Printing
EDS	Energy-dispersive X-ray Spectroscopy
FDM	Fusion Deposition Modelling
IM	Imidazolate
IMORF	Isoreticular Metal-Organic Framework
MMOF	Microporous Metal-Organic Framework
MOF	Metal Organic Framework
PE	Polyethylene
PCN	Porous Coordination Networks
PCP	Pulsed Current Processing
PVA	Polyvinyl Alcohol
PVB	Polyvinyl Butyral
PX	p-Xylene
OX	o-Xylene
SAPO	Silicoaluminiumphosphate
SEM	Scanning Electron Microscopy

SLA	Stereolitography
SLM	Selective Laser Melting
SLS	Selective Laser Sintering
XRD	X-ray Diffraction
ZIF	Zeolitic Imidazolate Framework
ZMOF	Zeolite-like Metal Organic Framework

1 Introduction

1.1 Framing and Project's Presentation

Nowadays, adsorption techniques play an essential role in the separation's processes. One of the highlighted fields where these techniques are applied is the separation of gases. In adsorptive separation when the solid (adsorbent), is exposed to a fluid, that contains the solute (adsorbate) there is adhesion of molecular species that are in the fluid phase to the surface of the adsorbent [1]. For this reason, due to the existence of different interactions between the molecules present in the fluid phase and the solid phase, adsorbents present distinct adsorption capabilities, thus allowing the separation of the gases [2].

Microporous materials, with a high surface area, are used as adsorbents. However, to have an excellent performance, that is, high thermal and mass transfer, low-pressure drop and high mechanical stability, they must be converted into hierarchically porous structures. Many materials, such as zeolites, metal-organic frameworks (MOFs), activated carbons, aluminium phosphates ($AlPO_4$s), silicoaluminiumphosphates (SAPOs), mesoporous silica, and hydrotalcites are used as adsorbents [3].

In this work, the shaping of ZIF-8 powder, purchased at Sigma-Aldrich (Basolite® Z1200), into pellets and monoliths and adsorption equilibrium isotherms of nitrogen (N_2) and methane (CH_4) in one of these materials were studied at 303 K. Besides, the chemical and morphological characterization of pellets and monoliths was performed. ZIF-8, with the chemical formula $C_8H_{10}N_4Zn$, is a zeolitic imidazolate framework (ZIF), that belongs to a new subclass of MOFs [4]. This crystalline material combines the characteristics of zeolites and MOFs and, for this reason, has unimodal micropores and a high surface area, making this material suitable for gas separation. Besides that, MIL-53(Al) powder, purchased at Sigma-Aldrich (Basolite® A100), was shaped into pellets and monoliths. The MIL-53(Al) pellets were characterized and adsorption equilibrium experiments using N_2 and CH_4 gases, in the material that presented the best set of properties, were performed at 303 K. MIL-53(Al), with the chemical formula $Al(OH)(C_8H_4O_4)$, is one of the most studied MOFs materials for adsorption applications.

The main interest of this work is to understand if the monoliths and the pellets, produced from ZIF-8 and MIL-53(Al) powders, present the properties needed to be used on a large scale gas separation, more specifically N_2/CH_4 separation, without leading to a significant loss in the adsorption capacity in relation to the original powder.

1.2 Outline

This work is divided into five chapters: introduction, context and the state of the art, materials and methods, results and discussion, and conclusions.

In the introduction, the aim of the work will be explained.

Context and the state of art chapter introduces some concepts essential for the realization and discussion of the results obtained. Special attention is given to MOFs, ZIFs and the technologies existent about powders shaping.

In the third chapter, the materials used in this work are briefly described. This includes the description of the powder adsorbents, the binders, and the solvents used to produce the shaped materials. Besides this, in this chapter the methods used to characterize the prepared samples, to characterize the ink used to produce the monoliths, to measure the mechanical strength of the materials, and to measure the adsorption equilibrium isotherms are concisely described.

After the description of the materials and the methods used, the results and its discussion were reported in chapter four. Firstly, the rheological characterization of the inks to produce the monoliths was presented. Then, the characterization of the shaped samples was also reported. To understand if the shaped materials had the mechanical strength necessary to be employed, a discussion about the crushing tests was done. Finally, adsorption equilibrium isotherms data is presented and discussed.

Finally, in the fifth chapter the main conclusions of this work are summarized, and an assessment of the developed work is done. This includes the achieved objectives and the future work that should be performed.

2 Context and the State of the Art

2.1 MOFs

In 1965, the first work about a new type of porous material, currently known as MOF, was published [5]. Since then, these materials have been studied and developed. Nowadays, MOFs are suitable for gas separation [6-9], purification [6, 7, 10], and gas storage [11, 12]. Besides these applications, MOFs have conquered space in other fields, as represented in Figure 1. This class of materials includes some subgroups, such as ZIFs [4, 13]; isoreticular MOFs (IMORFs) [14, 15], zeolite-like MOFs (ZMOFs) [16] and microporous metal-organic frameworks (MMOFs) [17].

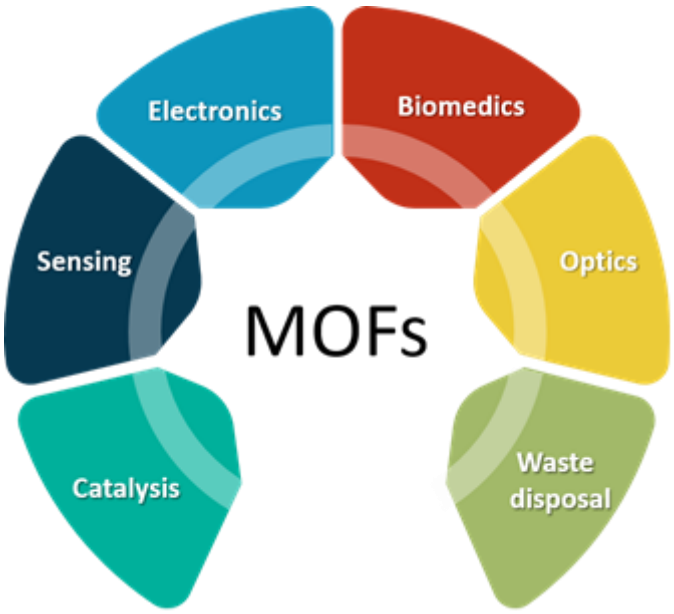

Figure 1 – Fields of application of MOFs.

These porous crystalline materials, with tunable pore sizes, possess single metal ions, which act as coordination centers, that are linked by organic ligands through, essentially, coordination bonds. There are many characteristics associated to MOFs, like their strong bonds, high surface area (up to 5000 $g \cdot m^{-2}$, and in rare cases over 6000 $g \cdot m^{-2}$ [18]), high void volumes (55-90 %) [14], the possibility of modification by organic synthesis and their high geometrical organization, typical of a crystalline structure . The organization of the crystalline zones is the feature that distinguishes MOFs from other porous materials like polymers or carbons [19]. The fact that these materials possess an organic and inorganic building block allows the existence of hydrophobic and hydrophilic species in the pores, which can change the adsorption properties of the material [20]. These characteristics are essential to make MOFs an essential class of adsorbent materials.

Contrary to the zeolites, MOFs, due to their properties and structure, can be well-design for a specific application through the cautious choice of the metal ion and especially of the organic ligand employed in the synthesis of the material, making MOFs tunable materials. The network connectivity of the MOF is what determines its properties, and in this way, by changing the organic linker or the inorganic part, MOFs with very distinct properties can be obtained. This means that although many of these materials are already discovered, there are still many to uncover, and consequently, there are many applications related to these materials in the field of adsorption to be studied. However, their thermal stability varies greatly from MOF to MOF, it is usually limited to 350-400 ºC, and rarely, to 500 ºC [21]. This must be taken into account when choosing a MOF for an application that requires high temperatures. In addition, some MOFs present a week chemical stability in the presence of water [22, 23], while others due to their hydrophobic behavior are stable in humid environments [24].

MOFs can be classified into two main classes: rigid and flexible [2]. The rigid ones have a fixed porosity, and for that reason hinder the entry of molecules with certain sizes and shape. On the other hand, flexible frameworks are influenced by the guest molecules, pressure, and temperature (leading to the modification of the structure of the MOFs), which can be an advantage over inorganic materials like zeolites. Besides this effect, the adsorptive separation occurred in MOFs can also be related to the strong or weak interactions between the fluid and the solid phase [8].

In the field of gas adsorption, the main applications of MOFs are related to the separation or storage of CO_2 , O_2, N_2 [25-27], H_2 [28, 29], CH_4 [6-9, 30], some hydrocarbons [7-9, 25, 26], carbon monoxide, CO, [7, 15, 25], some inorganic gases, [7, 31], noble gases [6, 26], water vapour [9, 10], other harmful gases [15] and solvent vapors [9, 14, 17]. In the case of CO_2, their high ratio between surface area and weight allows them to enhance the value of capacity in comparison to zeolites, at moderate pressures (> 10 bar) [32]. This way, MOFs have great chances to become essential in a wide range of separation/storage applications.

2.1.1 ZIFs

ZIFs are porous crystalline materials with a similar structure to the one of the zeolites. The transition metal zinc, Zn, or cobalt, Co, correspond to the atoms with tetrahedral coordination found in most zeolites and the imidazolate (IM) groups (nitrogenated organic linker) substitute the oxygen bridges [24]. An example of the type of linkage presented in ZIF molecules is represented in Figure 2. Like other MOFs, different organic ligands can give origin to many different types of ZIFs, which result in different adsorption properties.

Contrary to the generality of MOFs, these crystalline materials present high chemical stability in the presence of water [24, 33], due to the high basicity of the nitrogenated ligands [34]. This

fact makes ZIF materials suitable for applications in humid environments. In addition to water, some ZIFs are capable of resisting to some organic solvents [33] and basic media [24]. Besides that, the bond between the nitrogen of the ligand and the metal confers high thermal stability to ZIFs [33-35].

Currently, gas storage and separation processes are one of the main applications where these materials are employed. Adsorption studies, using ZIFS, of CO_2 [35-37], CO, N_2 [35, 36], Ar, CH_4 [35, 37], H_2 [37, 38], O_2 [33], solvent vapours [39, 40], hazard chemicals [40, 41], water vapour [40], some hydrocarbons [42-45] have already been made. However, it is expected that other accomplishments in this area will appear.

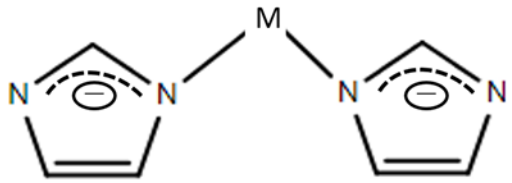

IM-M-IM

Figure 2 – Linkage present in ZIFs. M represents Zn or Co.

2.2 Shaping of Powders

The efficient shaping of a powder adsorbent/catalyst is essential for its scale-up, since it allows a lower pressure drop, keeping high mass, and thermal transference, improving the production rates and energetic efficiency in separation/storage industries [46].

To be structured into a resistant material, the powder must be subjected to some procedures. First, to become a mechanically stable material, the powder is commonly mixed with other constituents. Some examples of these components are binders, plasticizers, and solvents. Binders are used to allow that the final structure sticks together. Plasticizers make the mixture more flexible, assisting in this way the process of shaping.

On the other hand, solvents support this conversion of powder into a structured adsorbent/catalyst. It is noteworthy that these type of constituents result in a loss of capacity of the adsorbents since a large part of them do not have high adsorption properties. However, the advantages that the structuring of adsorbents provide compensates this loss of capacity. Once the mixture is made, it is then possible to start the shaping process. In this part, the powder is converted into the desired hierarchically porous structure. Lastly, the shaped material should be subjected to a thermal treatment to eliminate the guest molecules that are not part of the final material [3], and confer strength to the solid.

Adsorbents in the powder form bring issues to the adsorption process on a big scale. This way, shaped materials are the alternative and they can assume various structures, like extrudates [47, 48], tablets [49], laminates [50, 51], foams [52, 53], sheets [54], hollow fibres [55], spiral wounds [56], and monoliths [57, 58]. In particular, monoliths are structures that provide a better mass transfer and a low-pressure drop. However, the laminar flow of the gas could inhibit a good mixing of the fluid. In this way, the specifications of each monolith should be optimized according to the type of application [3]. Different techniques of shaping can form these final structures: tape casting, slip casting, gel casting, extrusion, coating, templating, foaming, spray drying, dry pressing, pulsed current processing [59, 60] and the emerging one, 3D printing.

Casting can be divided into three subgroups: **slip casting** [61], **tape casting** [62] and **gel casting** [63]. The colloidal suspension that will be cast could contain the porous powder, a liquid/polymer and other additives, such as, binders, dispersants, and others. The resultant slurry will be cast into a mold to form a hierarchical porous structure. In gel casting, the colloidal suspension solidifies in the mold and then is removed from the mold [63]. In case of slip casting the paste is placed in a plaster, with the desired shape and the reminiscent liquid is drained by the walls of the plaster mold. When the material is dried it can be removed from the mold [3, 61]. Lastly, tape casting consists in create a thin film from a liquid suspension [64].

In the case of the **extrusion** process, it is necessary to prepare a paste. This paste that is prepared in a mixer will consist of a mixture of the adsorbent powder, binder, solvent, and other optional components. The dough must present flexible properties to be extruded but at the same time show enough consistency in order to prevent the defects in the final product. In the process of extrusion, the prepared paste is pushed through a die. Concluded the shaping process, extrudates are obtained. Lastly, these extrudates will dry and be thermally treated. This technique is widely used to form pellets [47, 48] and monoliths [57, 58].

Coating is based on covering macroporous support, that usually has a high surface area, with micro/mesoporous active material. It is noteworthy that the active material could contain a binder and other additives, depending on the application. The substrate where the active part is deposited is what confers the mechanical stability to the final material. Besides that, the support in this type of application is essential for a good heat and mass transference and a low-pressure drop [65]. This technique allows the number of active constituents used in the coated-material to be lower than the one used in traditional pack beds, and usually presents higher surface areas [66]. There are already various studies made, employing some structures like monoliths [67, 68] or foams [52, 53] as support.

In **templating**, a solid or emulsion is used as a template to confer a certain shape or morphology to the final material. This method can give origin to materials with a wide range of porosities [3]. However, it is not possible to have a high volume of production with this technique [60].

Foaming is based on generating gas bubbles within a suspension that contains the active material [69]. After this procedure is done, the final foam is created by the drying of the resultant material. Contrary to templating this method allows a high production volume of final structures [60]. However, this method can lead to a low homogeneity, since there are two phases present with different densities. This way, the liquid one tends to go to the bottom of the material, and the gas one tends to go to the top, resulting in a higher porosity in the top of the final material [70].

In **spray drying** the concentrated fluid phase is sprayed into a drying element, which results in dried particulates. The final structures could be in the form of granules or agglomerates, and this will depend on the characteristics of the fluid phase and the shape of the drying element. This technique is very flexible in terms of production volumes [71].

Dry pressing consists in compressing a porous powder or a mixture of a porous powder and binder in a pellet press, which results in tablets or pellets. This technique does not involve elevated costs; however, it is not possible to obtain high production volume with this method. The resultant height and width of the obtained pellets/tablets depend on the pressure applied when pressing the material [72].

Pulsed Current Processing (PCP) is a binderless technique that allows the structuring of powder materials. Initially, the powder is packed in a die and is then submitted to a pulsed electrical current at the same time as a certain pressure is applied. The high heating rates allow fast thermal processing of the powders, which results in a partial fusion of these. This fusion results in a resistant material, without or with little quantity of binders [3, 73].

Lastly, **3D printing** is related to the print of a material in order to build a 3D body. A computer controls this process. In this technique, the object is created by adding layer upon layer of the material. The typical materials used in printing are powders, polymers, or metals. There are already many 3D printing techniques; some examples are fusion deposition modeling (FDM), robocasting, also known as direct ink writing (DIW), stereolithography (SLA), selective laser melting (SLM), and selective laser sintering (SLS). In FDM a polymer filament is heated to be extruded and added layer by layer [74]. In the case of DIW, a pseudoplastic paste is extruded by a nozzle that is moving in the platform of the printer according to the prototype defined in the computer. This method depends on the pseudoplasticity of the paste, while FDM depends on the solidification of the polymer [75]. The SLA method uses a liquid that through UV light is cured and solidifies according to the defined pattern. This process is repeated until the final structure is obtained [76]. SLS consists in using a powerful laser on a powder that results in its

sintering. To build the desired structure, the laser must be pointed at the powder according to a specific pattern. Once the first layer is finished another layer of powder is placed on top of the finished one. This process is repeated until the desired structure is obtained [75]. Finally, the SLM is quite similar to SLS, but instead of sintering, the material is melted.

Besides these methods, there are plenty of other ones.

As it has been mentioned before in most of the cases of shaping processes, a binder and a solvent are needed. For the production of pellets some systems of adsorbent/catalyst, binders, and solvents have been studied, some examples are presented in Table 1.

Table 1 – Examples of the studied systems to produce pellets.

Adsorbent/Catalyst	Binder	Solvent	Reference
Activated carbon	Sodium alginate	Water	[77]
TS-1 zeolite	Bentonite, silica gel, silica spheres, montmorillonite, sepiolite, methylcellulose	Distilled water	[78]
Zeolite Y	Alumina	Water	[79]
ZSM-5	Bentonite, silca, alumina, montmorillonite	Water	[80-82]
Zeolite 13X	Kaolin	Water	[83]
Zeolite CaX	Kaolinite	Water	[84]
Zeolite NaX	Kaolinite, hydromica	Water	[84]
Zeolite NaA	Kaolin clay, attapulgite, kaolinite	Water	[84, 85]
ZIF-8	Silica+portland cement+Methocel	Water	[86]
MIL-53(Al)	PVA	Water	[87]
MIL-101-Cr	PVB	Ethanol	[88]
HKUST-1	Alox C + graphite, PVA, PVB	Water, ethanol	[88-90]
Zr-MOF	Sucrose	Water	[91]
SIFSIX-3-Ni	PVB	Ethanol	[88]
SIFSIX-2-Cu-i	PVB	Ethanol	[88]
GeFSIX-2-Cu-i	PVB	Ethanol	[88]
TIFSIX-2-Cu-i	PVB	Ethanol	[88]
Mg-MOF-74	PVB	Ethanol	[88]

In order to produce monoliths using DIW technique, some mixtures have been studied. Examples of these mixtures are shown in Table 2.

Table 2 – Examples of works where the DIW technique was applied.

Adsorbent/Catalyst	Binder	plasticizer	Solvent	Reference
ZSM-5	Colloidal sílica+bentonite, Colloidal silica, Bentonite, Alumuminopphospate	Methyl cellulose	Water	[92-94]
MOF-74(Ni)	Bentonite clay	PVA	DI water+Ethanol	[95]
UTSA-16(Co)	Bentonite clay	PVA	DI water+Ethanol	[95]
Zeolite 13X	Coloidal sílica + bentonite + methyl celulose, bentonite + PVA	Methyl cellulose	Water, distilled water	[96]
Zeolite 5A	Bentonite + PVA	Methylcellulose	Distilled water	[96]
Aminosilica	Bentonite	Methylcellulose	DI water	[97]
SAPO-34	Graphite	Methyl Cellulose	Water	[98]
HZSM-5	Bentonite	Methyl cellulose	Water	[99]
Zeolite HY	Bentonite	Methyl cellulose	Water	[99]
Zeolite 13X+MCS-30 activated carbon	Carboxymethylcellulose	-	Distilled water	[100]

The use of adsorbents on an industrial scale continues to be an object of study because even though many adsorbents have significant adsorption capacities for certain components, they do not have the mechanical robustness necessary to be applied. This way, processes of structuring adsorbents must continue to be studied to take advantage of the useful properties of the adsorbents.

3 Materials and Methods

3.1 Material

3.1.1 Adsorbents

The first adsorbent used in this work was the powder of zeolitic imidazolate framework-8 (ZIF-8) (see Figure 3) acquired from Sigma-Aldrich. In this powder material, ions of Zn are linked by 2-methylimidozolate linkers through coordination bonds - Figure 3. This means that every atom of Zn is coordinated by four N atoms, which results in a tetrahedron [43]. The chemical formula of this material is $C_8H_{10}N_4Zn$, and it has a molecular weight of 227.58 g·mol^{-1}. Its pores with diameters of 11.6 Å are accessible through small apertures with a diameter of 3.4 Å [13].

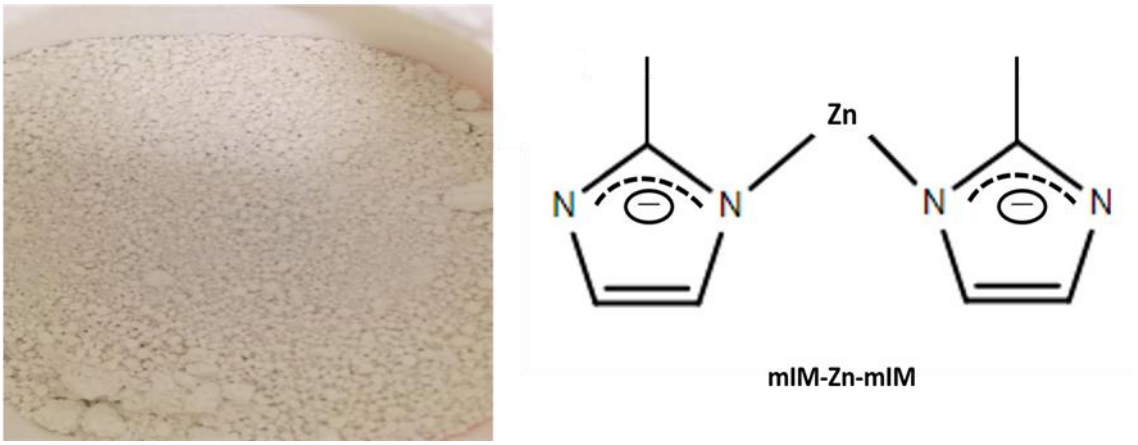

Figure 3 – Adsorbent powder (left) and type of linkage present in ZIF-8 (right).

The other adsorbent used was Matériau de l'Institut Lavoisier-53 (MIL-53), also known as aluminum 1,4-benzenedicarboxylate – Figure 4. This material that was discovered by the group of Ferey at Lavoisier Institute [20], with the chemical formula $Al(OH)(C_8H_4O_4)$ and with a molecular weight of 208.10 g·mol^{-1}, was purchased at Sigma-Aldrich. This porous solid has an aluminum ion as metal center and 1,4-benzenedicarboxylate (BDC) as the linker, generating 1D diamond shaped channels. MIL-53(Al) can undergo changes in the volume of its unit cells due to breathing effects. These effects, which make the structure go from a narrow pore one, with 19.5 x 7.6 Å^2 dimensions, to a large pore one, with 16.7 x 13.0 Å^2 dimensions [20], could be caused by diverse factors: pressure, temperature, and the interaction between adsorbent and adsorbate [101]. However, depending on the synthesis conditions , this breathing phenomena can be avoided [102]. Indeed, Heymans *et al.* [103] and Ferreira *et al.* [30] verified that the commercial powder, as well as, pellets of MIL-53(Al) provided by BASF, did not display the breathing behavior. These two structures can be observed in Figure 5. The hydration of the adsorbent causes hydrogen bonds to form between the oxygen atoms of the carboxylate groups

and the OH groups and the hydrogen atoms from the water molecules [104], resulting, this way, in a structure with narrow pores. It is noteworthy that CO_2 molecules could have the same effect; however, this effect could be reversed when high pressures are applied, opening, this way, the pores. In Figure 5 it is possible to observe the hydrated structure of this MOF (left) and the structure after the activation of the adsorbent (right), that is, its open form with large pores. In Figure 5 can also be observed the corner-sharing octahedral $Al(OH)_2O_4$ units linked by BDC groups.

Figure 4 – MIL-53(Al) powder.

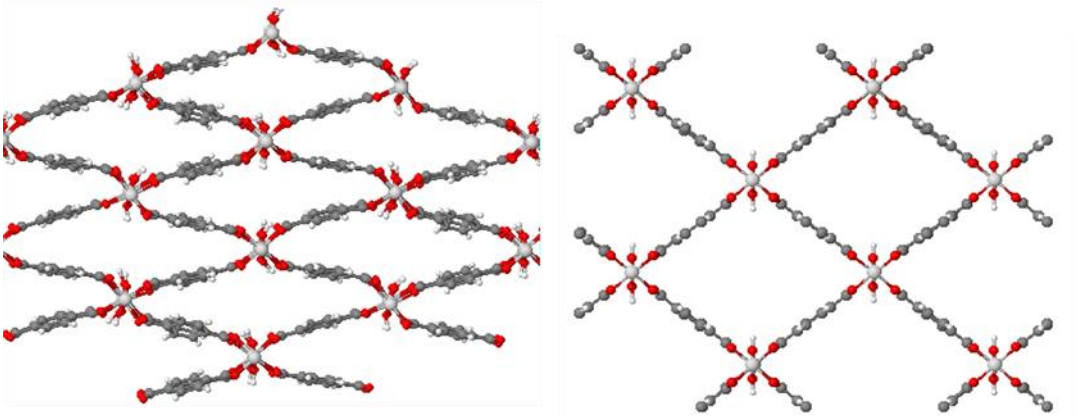

Figure 5 – The two structures of MIL-53(Al): structure with narrow pores (left) and structure with large pores (right).

3.1.2 Binders and Solvent

Aluminium oxide nanoparticles (see Figure 6 a)), Al_2O_3, known as alumina, purchased at ACS Material was used as a binder. This material was essential to guarantee that the final shaped material has the mechanical strength necessary for separation/storage applications.

Besides alumina, carboxymethylcellulose (see Figure 6 b)), CMC, acquired from VWR Chemicals, was also tested as a binder to provide some plasticity to the paste and at the same time promote the cohesion of the final material.

Lastly, kaolin (Figure 6 c)), purchased at VWR Chemicals, and polyethylene powder (PE - Figure 6 d)), acquired from Alfa Aesar, were used to produce the monolith constituted mainly by MIL-53-(Al). The first one was used to provide mechanical strength to the material, and the second one was used to confer flexibility to the paste.

Distilled water was used as a solvent, thus allowing the formation of an extrudable paste, since both adsorbents are water-stable [24, 105].

Besides distilled water, butanol was used to prepare a stable ink to produce the monolith containing MIL-53(Al).

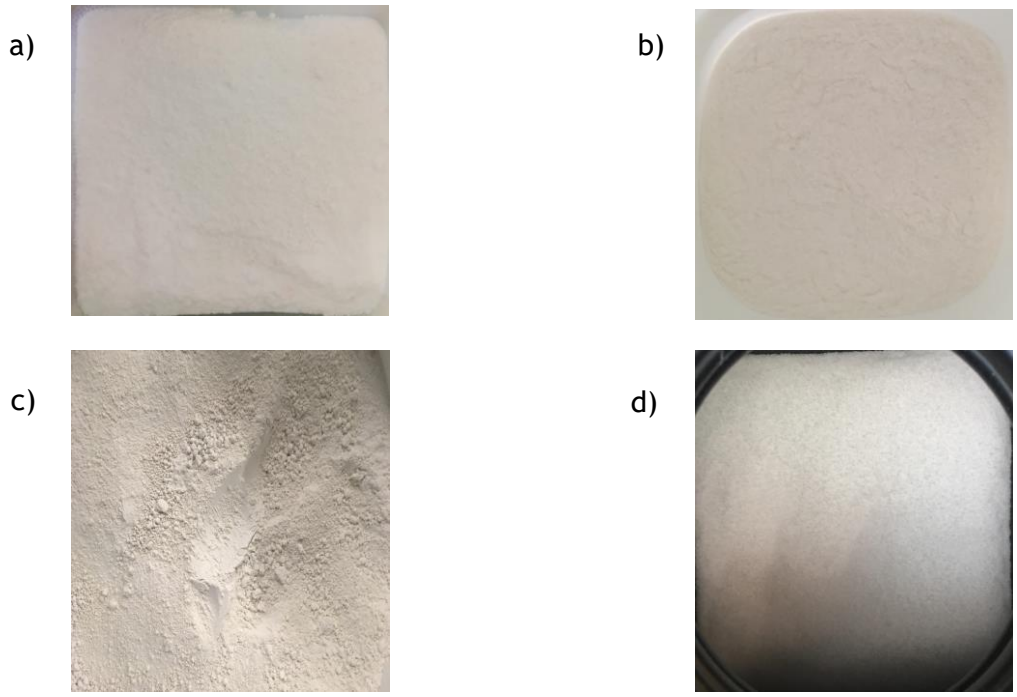

Figure 6 – a) alumina binder, b) CMC binder c) kaolin binder and d) PE binder.

3.1.3 Gases

In this work, adsorption properties of N_2 (≥ 99.999 %, Linde), CH_4 (99.95 %, Airliquide) were studied. Besides these two gases, helium (99.999 %, Airliquide), was used to do pycnometry experiments, and it was also used in the calcination treatment of the prepared shaped adsorbents.

3.2 Methods

3.2.1 Adsorbent shaping

In order to guarantee an excellent performance of the adsorbent, it is necessary to convert the powder into a structured material.

3.2.1.1 Adsorbent shaping into pellets

Pellets of ZIF-8 and MIL-53(Al) with different quantities of the binder were produced in Caleva Multi Lab extruder. This way, two binders were applied: alumina and CMC. In case of alumina, pellets with 5, 10 and 15 %wt. of this material were produced with both adsorbents, while with CMC, only pellets containing 5 and 10 %wt. of this binder were manufactured using ZIF-8 as adsorbent. The final pellets containing 5, 10 and 15 %wt. of alumina and produced with ZIF-8 will be named, from now on, as ZIF-8-PA5, ZIF-8-PA10 and ZIF-8-PA15, respectively, while the ones containing MIL-53 (Al) will be named MIL-53(Al)-PA5, MIL-53(Al)-PA10 and MIL-53(Al)-PA15, respectively. The ones containing 5 and 10 %wt. of CMC and ZIF-8 as adsorbent will be named ZIF-8-PC5 and ZIF-8-PC10, respectively.

Initially, the mixture of ZIF-8 or MIL-53(Al) powder and binder was prepared in the mixing chamber of Caleva Multi Lab extruder (Caleva Process Solutions Ltd, England) at room temperature. For the first 15-20 minutes, the defined mixing velocity was 40 rpm. Then, in the following 15-20 min, to guarantee the constituents were well mixed, the velocity value was increased to 60 rpm. To have an extrudable paste distilled water was added to the powder and binder mixture with a total dry mass of 5 g. The quantities of solvent needed in each case are presented in Table 3. In the mixing process, it was necessary to wait around 5 minutes after adding 1 mL of distilled water to guarantee a good mixture. Once the paste is made, the extrusion process was carried out. The velocities of extrusion needed in each case to extrude the material are also displayed in Table 3. In some cases, the velocity of extrusion was varied throughout the process, to guarantee that the paste had time to aggregate into extrudates and at the same time to ensure that the pellets would not have cracks. The die used in the process possesses holes with a diameter of 2 mm. This way, the extrudates obtained have the same diameter. Before the final thermal treatment, the pellets were dried at room temperature for about 24 hours to ensure slow evaporation of the water, preventing, in this way, the formation of cracks in the pellets. Finally, the calcination was made in an oven for 12 h while helium was being passed through the pellet samples. The operating temperature of the oven for each case is presented in Table 3. It is noteworthy that ZIF-8 is thermal stable up to 823 K, while MIL-53(Al) starts decomposing at 773 K [101]. In relation to binders, CMC does not have a good thermal stability (up to 300 K), and alumina only starts decomposing at very high temperatures [106].

Table 3 – Quantities of solvent, velocity of extrusion and temperature of calcination needed in order to produce the pellets.

	ZIF-8					MIL-53(Al)		
	PA5	PA10	PA15	PC5	PC10	PA5	PA10	PA15
Solvent (mL)	5	5	6	5	5	7	7	8
Velocity of Extrusion (rpm)	25	40	25	10	15	15-20	15-20	15-20
Calcination Temperature (K)	573	573	573	523	523	573	573	573

3.2.1.2 Adsorbent shaping into monoliths

Monoliths with 5 and 10 %wt. of CMC using ZIF-8 as adsorbent and MIL-53(Al) monoliths containing 5 %wt. of kaolin and 5 %wt. of PE were produced through DIW technique using an Ultimaker 2Plus printer (Figure 7 a)), which was coupled with a Discov3ry Extruder module acquired from Structur3D Printing, Canada - Figure 7 b). The resultant monoliths containing 5 and 10 %wt. of CMC will be named ZIF-8-MC5 and ZIF-8-MC10. The monolith of MIL-53(Al) will be named from now on MIL-53(Al)-M.

a) b)

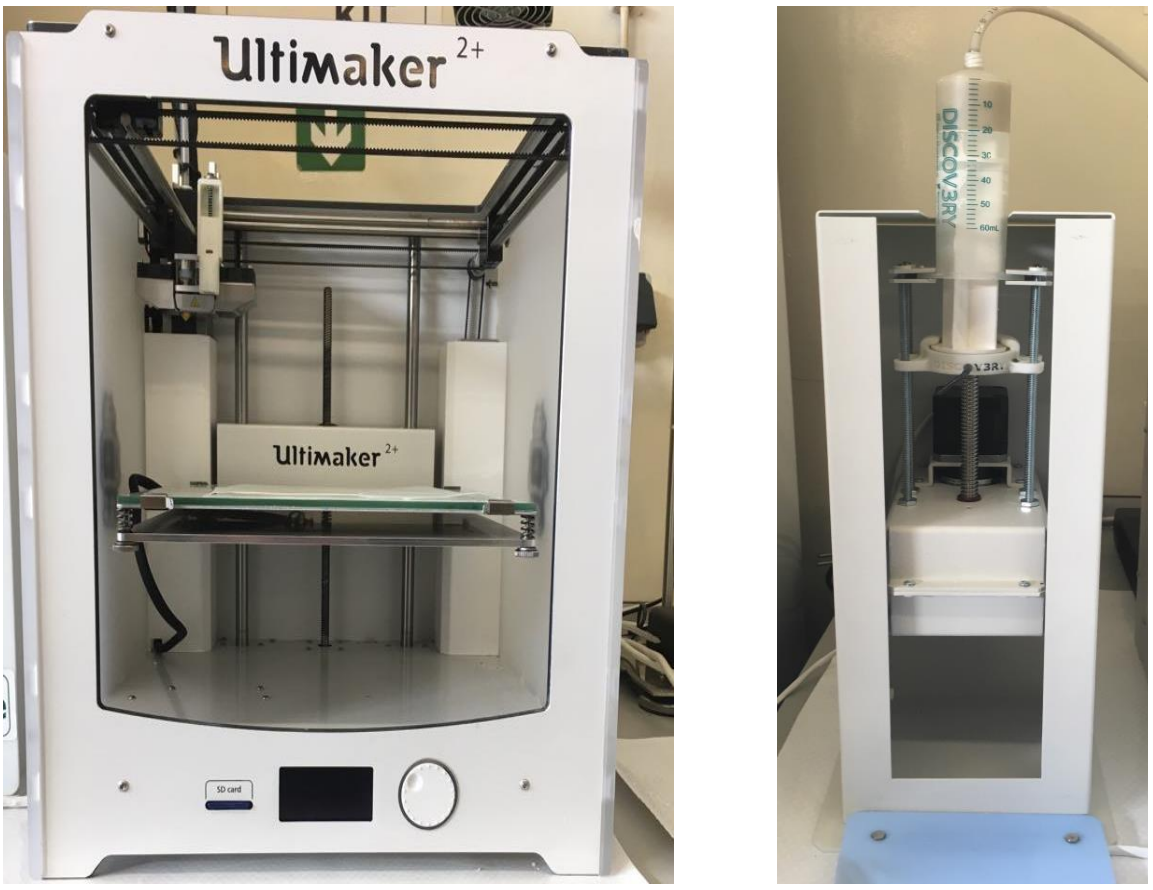

Figure 7 – a) Ultimaker 2Plus printer and b) Discov3ery Extruder module.

Initially, the design of the monolith was defined using the SolidWorks 2017 software. Then, with Ultimaker Cura 3.1.0 software a G-code program was generated which allowed to set the

printing parameters desired and visualize the design developed. The design can be observed in Figure 8.

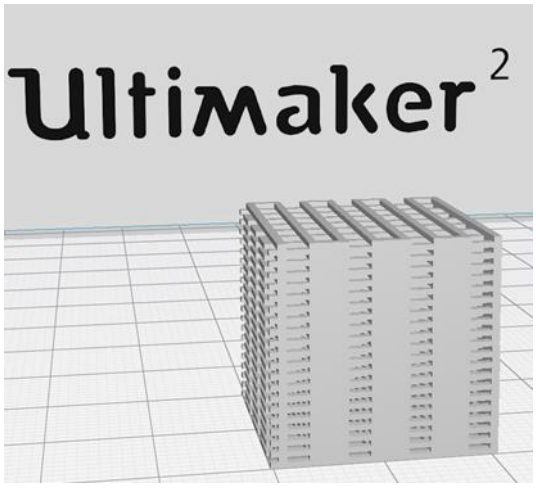

Figure 8 – Design of the monolith visualized in Ultimaker Cura 3.1.0.

Just as occurred with the pellets, first, it was necessary to prepare the paste, also called ink. The procedure of this preparation was similar to the one used with pellets, but instead of using 5 g, 15 g were used. This way, to have a printable paste DI water was used to produce the inks containing ZIF-8, and butanol was used to produce the ink with MIL-53(Al). The volumes of the solvent used to produce the inks are summarized in Table 4.

Once the ink is prepared, it is deposited in a syringe which subsequently is positioned in a Discov3ry Extruder module (see Figure 7b)).

In the printing step, the plunger of the syringe is pressed by a screw that was previously adjusted. This pressure will allow the ink to be pushed up to the nozzle, wherein the connection between the syringe and the nozzle is made by a plastic tube. This nozzle, with 1.54 mm orifice, through which the paste comes out, moves along the axis xx, yy and zz as programmed.

The drying process occurred at room temperature for ZIF-8-MC5 and MIL-53(Al)-M. For ZIF-8-MC10 a colder environment was provided to ensure that the material did not dry too fast. Besides that, the plate was kept cold for "ZIF-8-MC10" during the printing process.

Table 4 - Summary of the volume of solvent used to produce the inks.

	ZIF-8-MC5	ZIF-8-MC10	MIL-53(Al)
Solvent (mL)	17	18	28

3.2.2 Characterization

3.2.2.1 Rheological Properties

Before printing the monolith, it was necessary to evaluate the rheological properties of the paste, to find out if this one had the right properties to be printed. The paste must present

sufficiently high yield stress to resist deformation after being printed. Besides that, the viscoelastic ink must demonstrate a pseudoplastic behavior, this is, the viscosity should decrease with the increase of shear rate. This type of behavior will facilitate the deposition of the ink.

The rheological tests were performed in a rheometer (see Figure 9) from Anton Paar GmbH MCR 92, Austria. This rheometer presents a plate-plate geometry and it is controlled by software RheoCompass™ V1.20.496. The diameter of the plate used is 50 mm, and the gap between them during the tests was 0.5 mm for the pastes containing ZIF-8 and 1.0 mm for the ink of MIL-53(Al). All the tests were carried out at 298 K. Seven pastes were tested: ZIF-8 ink containing 15, 35, 50, and 75 %wt. of alumina, ZIF-8 paste having 5 and 10 %wt. of carboxymethylcellulose, and the MIL-53 ink with 5 %wt. of kaolin and 5 %wt. of PE.

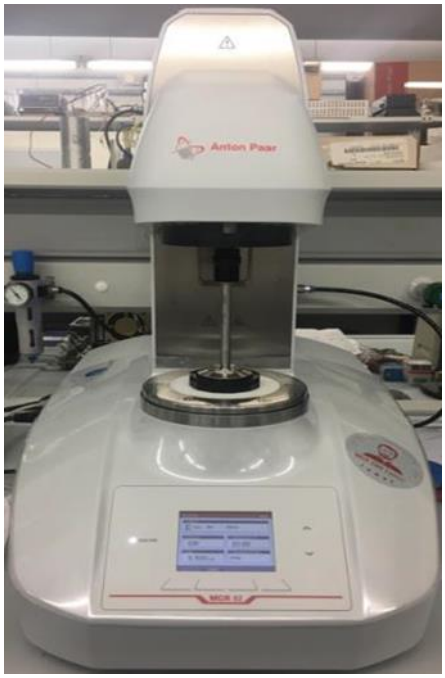

Figure 9 – Rheometer Anton Paar GmbH MCR 92.

First, rotational tests were made to observe the variation of the viscosity with the increase of shear rate. These tests were performed by imposing a logarithmic ramp increase to the shear rate value. The range of shear rates imposed varied according to the ink which was being analyzed. Then, oscillatory tests, more specifically, amplitude sweep tests, were performed at a constant frequency equal to 1 Hz. These tests allow the observation of the viscoelastic behavior of the ink, namely the variation of storage modulus (G') and the loss modulus (G'') with the increase of the strain or shear stress. A logarithmic ramp increase was applied to the value of strain and the range of strain values was varied according to the paste that was being analyzed, in order to observe correctly the strain at which G'' became greater than G'.

3.2.2.2 Scanning Electron Microscopy (SEM) with Energy-dispersive X-ray Spectroscopy (EDS)

SEM/EDS analysis of ZIF-8 powder, ZIF-8-PA5, ZIF-8-PA10 and ZIF-8-PA15 were performed in Centro de Materiais da Universidade do Porto (CEMUP) using FEI Quanta 400FEG ESEM / EDAX Genesis X4M, operating at an acceleration voltage of 10 or 15 kV depending on the sample that was being analyzed. To produce the micrographs, the sample that is being observed must be conductive, and for that reason, the samples were coated with a thin film of gold/palladium, by sputtering, using the SPI Module Sputter Coater equipment.

3.2.2.3 Textural Characterization

Textural characterization was performed in all the samples, including the adsorbent powders, with exception of MIL-53(Al)-M, at the University of Málaga by using three techniques: N_2 adsorption at 77 K, CO_2 adsorption at 273 K, and mercury porosimetry. Before proceeding to the measurements all the samples were activated at 423 K under vacuum.

N_2 and CO_2 adsorption isotherms measurements were carried out using a Micromeritics ASAP 2420 Accelerated Surface Area and Porosimetry System (USA) at 77 and 273 K, respectively. This way, by analyzing the adsorption experiments with N_2, it was possible to determine the specific surface area and the micropore volume of the samples. With CO_2 adsorption measurements, it was to possible to calculate the volume of pores with a diameter lower than 7.97 Å.

Mercury porosimetry was used to observe the macropores size distribution, as well as the macropores average diameter, and the apparent density. Hg porosimetry measurements were performed up to a pressure of 206.5 MPa and were obtained using a Micromeritics' AutoPore IV 9500 Series (USA).

3.2.2.4 X-ray diffraction (XRD)

The crystalline structure of the ZIF-8 powder, MIL-53(Al) powder, and the shaped samples, excluding MIL-53(AL)-M were observed in Servicios Centralizados de Apoyo a la Investigación (SCAI) of Universidad of Málaga using an EMPYREAN diffractometer (PANalytical), with $CuK\alpha_{1,2}$ radiation from 5.0º to 80.0º. Before starting the measurements, all the shaped samples were reduced to powder.

3.2.3 Mechanical Strength Tests

Mechanical strength tests were performed on the all pellet samples containing alumina using a type 5Y hardness tester (Pharmatron/Dr. Schleuniger, Delft). The measuring range utilized was of 2-400 Newton. Fifty particles of each sample were tested.

3.2.4 Adsorption Equilibrium Isotherms

The adsorption equilibrium isotherms of CH_4 and N_2 in ZIF-8-PA5 and MIL-53(Al)-PA5 were measured at 303 K to analyze the adsorption properties of the adsorbents. The measurements were done using a magnetic suspension balance (MSB, Rubotherm®, Bochum, Germany) which has a 0.01 mg precision. Before starting the measures, the samples were activated at 423 K under vacuum for 12 hours. In Figure 10, a scheme of the experimental set-up can be observed.

Besides the MSB, the system is constituted by five valves, a thermocouple, three pressure transducers, and a vacuum pump. The last one allows the depressurization of the cell and the activation of the samples. The valves grant the possibility of connection of the gas bottle to the cell, allowing the entrance of adsorbate in the cell. Besides this, the valves also link the vacuum pump to the cell. The thermocouple and the pressure transducers are present to monitor the temperature and the pressure inside the cell, respectively. One of the pressure transducers is used for pressures below 0.35 bar, the second one is used at pressures between 0.35 and 10 bar, and the last one is used when the measurements are performed at a pressure higher than 10 bar and lower than 200 bar. This way, it is possible to obtain high rigor in the pressure values. The provided Rubotherm software does the data acquisition and system control. The variation of temperature is controlled through electric resistance.

Before starting the measurements, the adsorbent was weighed and inserted in a basket that was linked to the permanent magnet. Through the attraction forces between the permanent magnet and the electromagnet, it is possible to measure the mass variations inside the cell and to record them in the acquisition system.

In these experiments, the measured mass has to be corrected due to the buoyancy effect. This way, assuming that helium is not adsorbed, three helium pycnometry experiments were performed, one where the system was constituted by the basket, the permanent magnet, the glass wool, and the suspension shaft and the other two constituted by the same things plus each one of the adsorbents. The results obtained for helium pycnometry experiments are reported in Appendix A. Lastly, to calculate the absolute amount adsorbed, the buoyancy was corrected according to the following the Equation 1:

$$q = \frac{\Delta m + \rho_{\mathrm{G}}(V_{\mathrm{s}} + V_{\mathrm{c}})}{m_{\mathrm{s}} M} \frac{\rho_{\mathrm{ads}}}{\rho_{\mathrm{ads}} - \rho_{\mathrm{G}}} \qquad \text{Equation 1}$$

In the Equation 1, Δm is the difference between the measured weight and the weight when there is no gas in the cell, ρ_{G} is the density of the gas phase at the pressure and temperature registered in the measurement, V_{s} is the volume of the solid adsorbent, V_{c} is the volume of the basket, the permanent magnet, the glass wool and the suspension shaft, ρ_{ads} is the density of

the adsorbed phase at the measuring conditions, m_s is the mass of solid adsorbent and M is the adsorbate molecular weight.

To measure each point of the isotherm, gas was introduced in the system, and equilibrium was achieved when the corrected weight measured by the system did not vary. This procedure was repeated until all desired points of pressure were obtained.

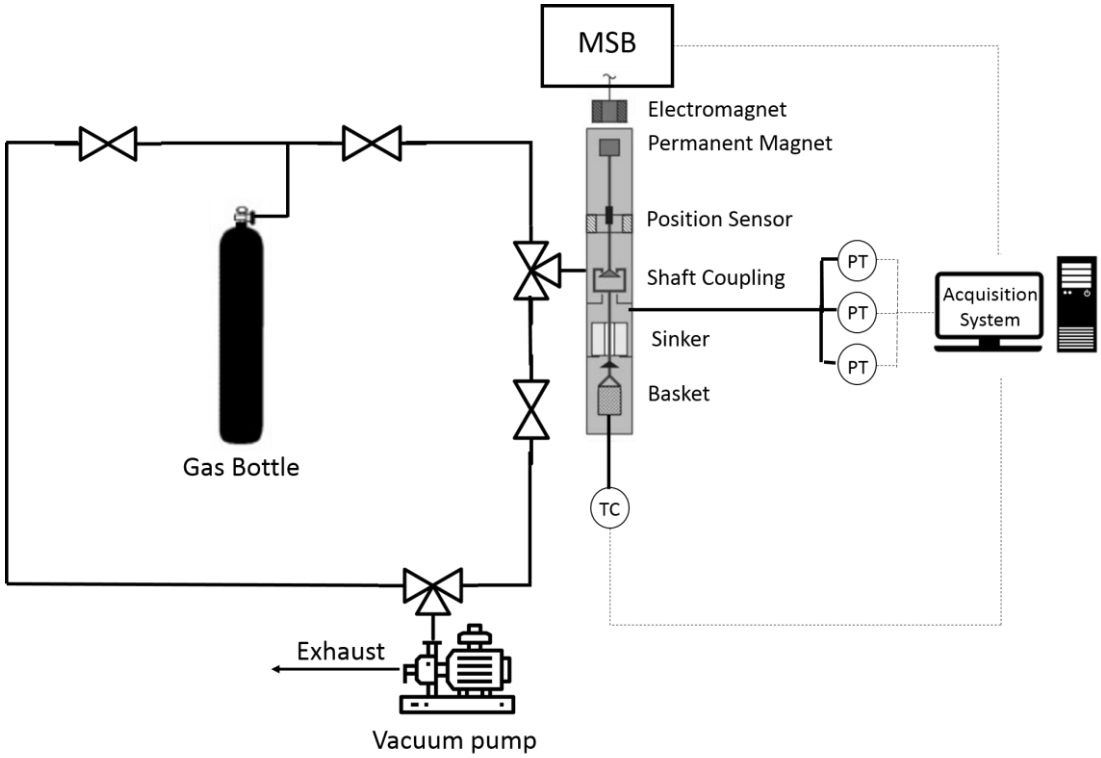

Figure 10 – Diagram of the experimental set-up used for adsorption equilibrium measurements.

4 Results and Discussion

4.1 Rheological behavior of the printing paste

In order to ensure that the paste has the right properties to be printed, its rheological behavior must be studied. This way, the viscosity was plotted as a function of shear rate for all the pastes studied to produce the monoliths. The viscous behavior of the inks containing ZIF-8 and alumina and for the ones containing ZIF-8 and CMC can be observed in Figure 11. For the MIL-53 ink, the same study was done, and the results can be observed in Figure 12.

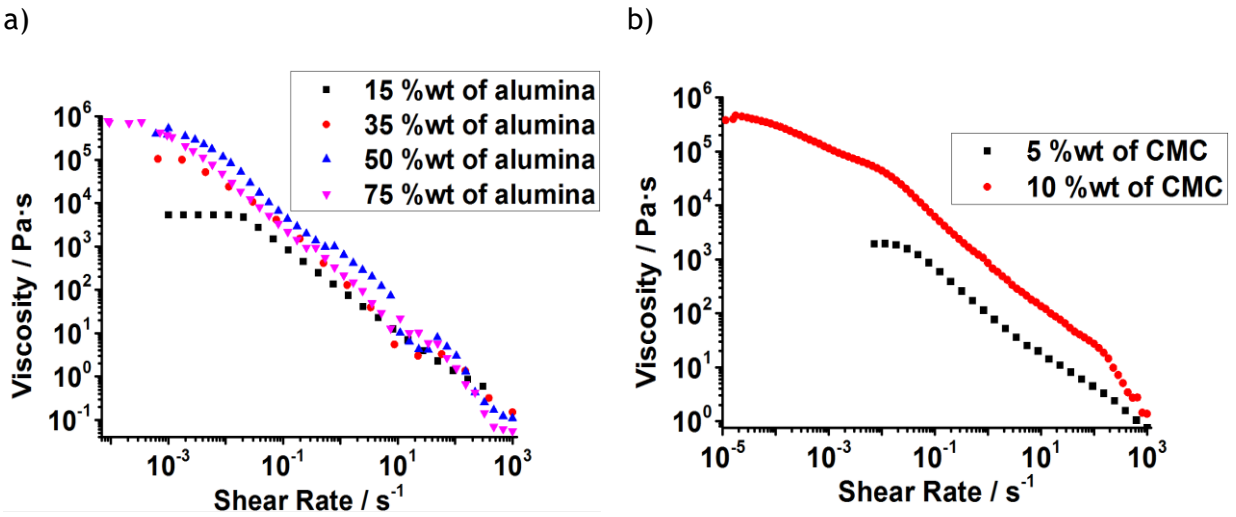

Figure 11 – Variation of viscosity with the shear rate for the inks containing ZIF-8 and a) alumina, b) CMC.

To print a monolith, it is necessary to observe a pseudoplastic behavior, this is, the viscosity of the ink must decrease when the shear rate increases [107]. This will enable an easier extrusion and deposition of the ink. Initially, it is expected that pseudoplastic materials have a constant viscosity for lower shear rates; this value of viscosity is called zero-shear viscosity and corresponds to the Newtonian plateau. Then, with the increase of shear rate, the initial viscosity plateau evolves to a shear thinning zone, where the viscosity decreases with the rise of the shear rate. Lastly, at very high shear rates, a plateau could be obtained again, this value of viscosity is called infinite-shear viscosity [108].

As it is possible to see, for all the inks a shear thinning behavior could be observed (Figure 11 and Figure 12), pointing, this way, that the pastes seem to have the right viscous properties to be printed. For all the inks it is possible to observe a Newtonian plateau for low shear rates, this is, a plateau where the viscosity is constant (η_0), which constitutes a proportionality between the shear stress and the shear rate. This plateau is described by Newton's law [108]. In relation to the value of η_0, for the inks containing ZIF-8, the higher the amount of binder the higher the η_0, due to the greater resistance for the paste to flow.

For the pastes containing ZIF-8 and alumina (see Figure 11a)) as the shear rate increases the viscosity of the inks with different contents of binder become quite similar. This can be proven by the overlap of the curves of the pastes containing 35 %wt. up to 75 %wt. of alumina, for the shear rate values for which the pseudoplastic behavior is observed. Looking close to the viscosity curves, it is easy to detect that for higher values of shear rate, the values of viscosity become identical

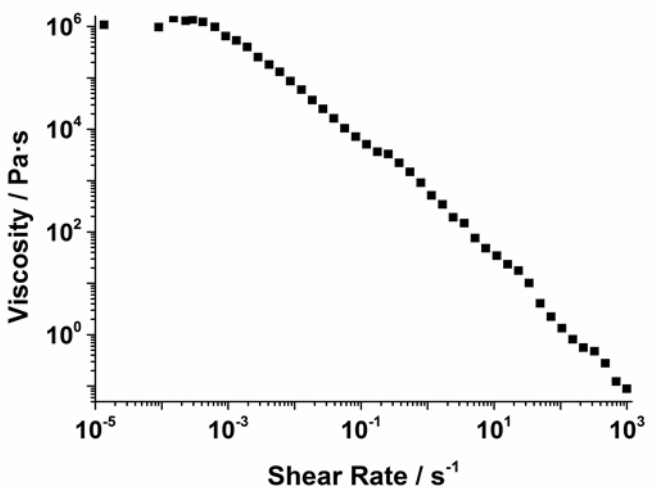

Figure 12 - Variation of viscosity with shear rate for the ink with MIL-53(Al).

With respect to the paste containing CMC (Figure 11b)), the values of viscosity in the transition zone are quite distinct, however, for the higher values of shear rate, the viscosity values become a bit similar, like what happens with the final values of viscosity registered for the ZIF-8 + alumina ink.

The inks have different behaviors and, for this reason, there are certain models that suit better the experimental data than others. Indeed, to explain the viscosity data of pseudoplastic inks, two mathematical models are usually applied: Cross' model (Equation 2) and Carreau's model (Equation 3). These equations are presented below:

$$\frac{\eta_0 - \eta_\infty}{\eta - \eta_\infty} = \frac{1}{(1 + k\dot{\gamma})^m} \quad \text{Equation 2}$$

$$\frac{\eta_0 - \eta_\infty}{\eta - \eta_\infty} = \frac{1}{(1 + (k_1\dot{\gamma})^2)^{\frac{m_1}{2}}} \quad \text{Equation 3}$$

where η_0 is the zero-shear viscosity and corresponds to the value of the Newtonian plateau, k and k_1 are the transition times, m and m_1 are the viscosity exponents, $\dot{\gamma}$ is the shear rate, η_∞ is infinite-shear viscosity and η is the viscosity.

Figure B.1 and Figure B.2 (Appendix B) show the fit of the mathematical models to the experimental results for the pastes with ZIF-8 and the paste containing MIL-53, respectively. As it can be seen the two mathematical models represent well the experimental data at low and high shear rates. The parameter values of the models can be seen in Table 5.

As expected, for the inks containing the same constituents the value of η_0 is higher for the pastes containing a higher amount of binder. Another aspect that must be noticed is the fact that for all the pastes the two mathematical models can be used. However, it looks that the Cross' model is better to predict the behavior of the inks with the higher viscosity and the Carreau's model the paste with lower viscosity. Besides that, none of the inks, at the range of shear rate tested, presented a plateau corresponding to the infinite-shear viscosity.

Table 5 - Parameters of the mathematical models used to describe the viscous behavior of the inks.

	ZIF-8						MIL-53
	+15 %wt. of alumina	+35 %wt. of alumina	+50 %wt. of alumina	+75 %wt. of alumina	+ 5 %wt. of CMC	+ 10 %wt. of CMC	+ 5 %wt. of PE + 5 %wt. of kaolin
η_0 (Pa·s)	$5.5x10^3$	$1.1x10^5$	$5.3x10^5$	$7.9x10^5$	$1.9x10^3$	$4.2x10^5$	$1.2x10^6$
k (s)	48	214	345	1193	54	1800	1002
k_1 (s)	55	229	390	1330	55	2742	1077
m	1.0	1.2	1.2	1.2	0.7	0.8	1.2
m_1	1.0	1.2	1.2	1.2	0.7	0.8	1.2
η_∞ (Pa·s)	0	0	0	0	0	0	0

For the pastes with alumina, it is possible to observe that for the pastes with lower amount of the binder the difference between the values of η_0 is more accentuated than for the pastes with higher amount of the binder. This can be easily noted when comparing the values of zero-shear viscosity of the pastes containing 15 %wt. of alumina and 35 %wt. of alumina ($5.5x10^3$ vs $1.2x10^5$) and then comparing the ones of the pastes with 50 %wt. of alumina and 75 %wt. of alumina ($5.3x10^5$ vs $7.9x10^5$). This way, as the amount of binder is increased, this increase becomes less important to change the initial properties of the ink. The m and m_1 values are related with the shear thinning region, *i.e.*, these values represent the viscosity's dependence on the shear rate. By observation of Figure 11 a) it is possible to notice that for the three pastes with the higher content of binder the shear thinning area is similar, this way, the values of these parameters are the same. However, for the paste that contains 15 %wt. of alumina, the exponent value is lower due to a minor viscosity's dependence on the shear rate. The fact that the viscosity of the inks with higher amounts of binder present a higher dependence on the shear rate could be related with the number of entanglements, the higher the number of entanglements the higher the impact of an increase in the shear rate in the disentanglement of the molecules [109]. It is possible to observe (see Figure 11a)) that for these pastes the minimum shear rate for which the viscosity starts to decrease is different. This is strictly connected to the k value of the mathematical models, the higher the transition time value, the lower are the shear rates at which the shear thinning behavior starts to occur [110]. This way, as expected by the observation of Figure 11 a), the higher the content of the binder in the paste, the higher the k values (see Table 5).

By analyzing the parameters' values for the pastes containing CMC, it is possible to infer that a change of 5 %wt. of binder results in significant changes in the paste's properties. This can be observed by comparison of the η_0 values, for the paste containing 10 %wt. of CMC the zero-shear viscosity is almost two hundred times greater than the one of the 5 %wt. of CMC ink. The differences between the values of the viscosity exponents and the transition times of the pastes with CMC have the same explanations than the ones that are presented for the pastes containing alumina.

The paste with MIL-53(Al) is the one that presents the higher value of η_0. The transition time value is similar to the ones presented for the pastes containing the three higher amounts of alumina, thus showing that the viscosity behavior of this paste has the same dependence on the shear rate than the referred pastes with alumina.

Besides rotational tests, amplitude sweep tests were performed in all the inks. This type of tests allows evaluating the variation of the G' and G'' with the increase of the strain or the shear stress. The G' value is associated with the elastic behaviour of the ink, *i.e.*, with the capacity of the ink to recover from a deformation. For that reason, this parameter represents the solid-like behaviour of the ink. The G'' value is related to the viscous behaviour of the ink, this is, when a deformation is applied, the ink cannot recover its initial position. Therefore, this parameter expresses the liquid-like behaviour of the paste. Indeed, for a certain temperature and frequency, it is possible to understand which behaviour of the ink is predominant at a certain shear.
To produce monoliths, it is necessary that the pastes possess a high gel point, *i.e.*, the paste only starts to behave predominantly like a liquid when a specific value of strain is applied. This allows that after being printed the paste resists to deformation.
Figure 13 and Figure 14 show the variation of G' and G'' with the strain for the pastes containing ZIF-8 and MIL-53(Al), respectively.

For all the pastes, it is possible to observe that initially, at lower strains, the G' values are higher than the G'' values. With the increase of the strain, the values of both moduli start to decrease. However, the G' value decreases more rapidly than the G'' value, and for a certain value of strain the G'' value becomes higher than the G' value, thus showing that the molecules of the paste are losing the capacity to store energy. This demonstrates that the inks have a change in the behavior, switching from a predominant solid-like behavior (elastic) to a predominant liquid-like behavior (viscous). This ability of the pastes to present elastic and viscous properties when a strain is applied is typical of a viscoelastic material. The strain (γ_g) for which the G'' values become higher than G' values it is called gel point, which means that the viscous part dominates and the paste flows. These values are presented in Table 6.

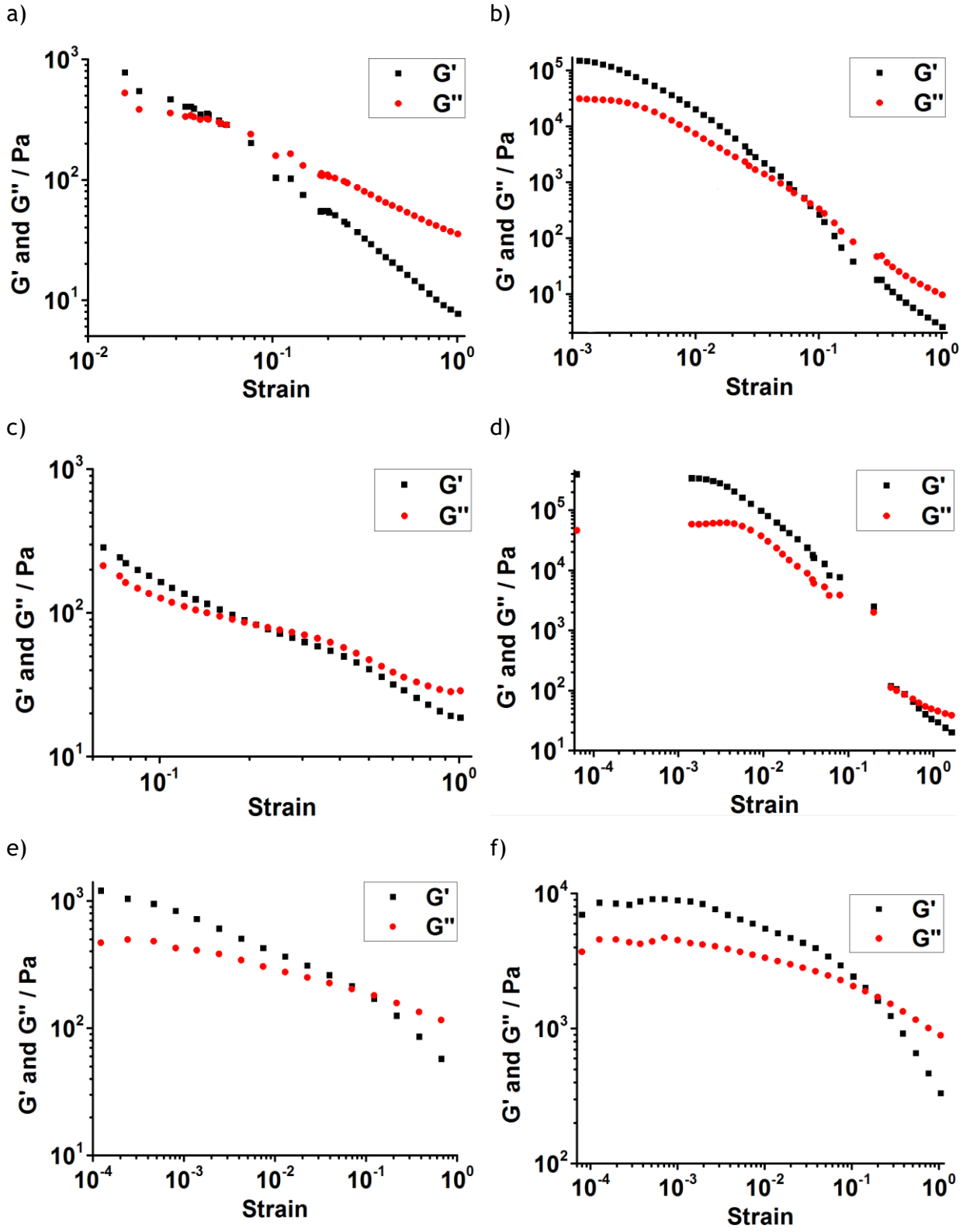

Figure 13 - Storage and Loss modulus of the pastes of ZIF-8 and a) 15 %wt. of alumina, b) 35 %wt. of alumina, c) 50 %wt. of alumina, d) 75 %wt. of alumina, e) 5 %wt. of CMC and f) 10 %wt. of CMC.

This is related with the printing process since when the pressure applied or the strain applied is low, the ink has a predominant elastic behavior given that the molecules of the material are entangled and for that reason, the paste cannot be printed through the nozzle. When the pressure applied increases to the point where the molecules align themselves along the flow

direction, the ink starts to flow, and it is then possible to print the ink. Finally, when the paste has already been printed there is no strain or stress applied on it, and therefore it recovers its solid-like behavior partially and can resist to deformation.

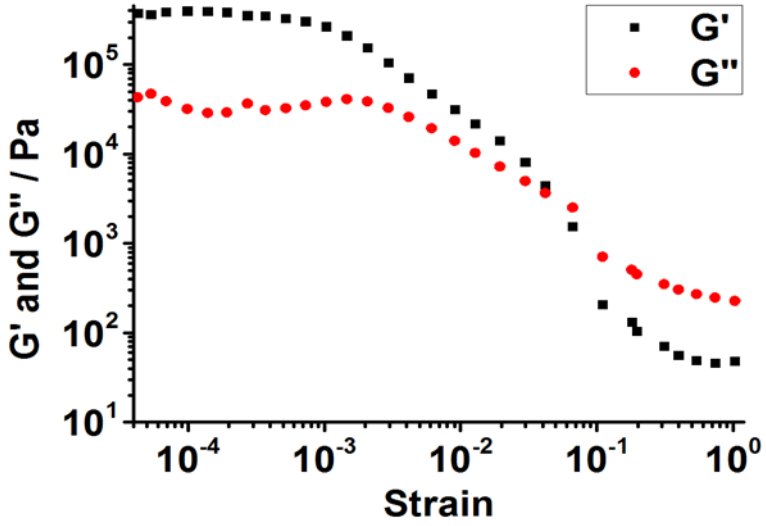

Figure 14 - Storage and Loss modulus for the paste containing MIL-53.

Table 6 - Summary of the important values of the amplitude sweep tests.

	ZIF-8						MIL-53
	+15 %wt. alumina	+35 %wt. alumina	+50 %wt. alumina	+75 %wt. alumina	+ 5 %wt. CMC	+10 %wt. CMC	+ 5 %wt. PE + 5 %wt. kaolin
G' in LVR (Pa)	-	-	-	$3.6\text{x}10^{5}$	-	$8.9\text{x}10^{3}$	$3.8\text{x}10^{5}$
G'' in LVR (Pa)	-		-	$5.4\text{x}10^{4}$	-	$4.4\text{x}10^{3}$	$3.6\text{x}10^{4}$
γ_L	-	-	-	$2.1\text{x}10^{-3}$	-	$1.9\text{x}10^{-3}$	$3.7\text{x}10^{-4}$
γ_G	$5.6\text{x}10^{-2}$	$7.6\text{x}10^{-2}$	$2.1\text{x}10^{-1}$	$4.6\text{x}10^{-1}$	$7.0\text{x}10^{-2}$	$2.0\text{x}10^{-1}$	$4.2\text{x}10^{-2}$

For some pastes it is possible to distinguish a linear viscoelastic region (LVR) where the G' modulus values are constant for low values of strain (see Figure 13 d) and f) and Figure 14). On the rest of the pastes, this region is not observed due to the elevated deformation that the pastes already had at the chosen frequency, meaning that the initial forces present on the inks had weakened and the material had already started to flow irreversibly. The strain range is not the same to all the tests given the limited time for the rheometer use, therefore was not possible to assess the LVR region for all the pastes. If the tests had been performed using the same strain range, it would be expected that the pastes with the same components and higher binder amount had higher moduli' values in the LVR. In this region, the material maintains its properties independently of the shear stress or strain applied. For this reason, to obtain a printable paste, the strains applied on the inks must be bigger than the range of strain of LVR. For these pastes, it is possible to observe the limiting value (γ_L) of the inks, *i.e.*, the value of shear stress/strain for which the G' values start to decrease due to the weakening of the

structural strength of the pastes. These values correspond to the strains where the G' values are 90 % of the value of G' in the LVR [111] and the obtained values are reported in Table 6.

When comparing the pastes with the same components, it is possible to notice that with the increase of the binder quantity, the gel point becomes also higher. This means that for the inks with a higher amount of binder, it is necessary to apply a higher deformation before the paste starts to flow. Besides that, the binder helps the paste to recover partially its elastic behavior faster, which is an essential feature of ink to be used in 3D printing.

In the open literature, there are tests performed with two different pastes, one containing alumina [107], and other containing zeolite, activated carbon and CMC [100] and the reported results are in good agreement with the results obtained in this work.

These tests are essential to understand if the paste has the right rheological properties to be printed, like a pseudoplastic behavior and a sufficiently high gel point. However, there are no defined values for the rheological parameters that the paste must have to be printed. In this way, these tests are a screening of the inks that go to the stage of 3D printing, yet not knowing for sure if this step is going to be successful or not.

Finally, it is recommendable that all the tests performed had been repeated more than once but considering the defined deadlines and the availability of the equipment, only one measurement for each paste was done.

4.2 Adsorbent shaping

4.2.1 Pellets

To ensure that the produced pellets are homogeneous and have a suitable mechanical strength, the shaping process is essential. First, to guarantee that the pellets are homogeneous the components must be well mixed. To obtain pellets with high mechanical strength, the right quantity of water must be added to the mixture, and a thermal treatment must be done to ensure that the final material is dried.

The first step to shape the adsorbent into pellets is to obtain a mixture with the desirable properties to be extruded. The appearances of the pastes obtained for the pellets containing ZIF-8 + alumina, ZIF-8 + CMC, and MIL-53 are presented in Figure 15. The ZIF-8 + CMC paste (Figure 15 b)) has a “wet” appearance that is not expected for this type of shaping. However, when trying to make this process with less water the paste dried very fast on the screw clogging the dye, even getting a burned appearance. Besides that, the pastes containing ZIF-8 + CMC and MIL-53(Al) + alumina have a more plastic appearance which does not favor the extrusion process.

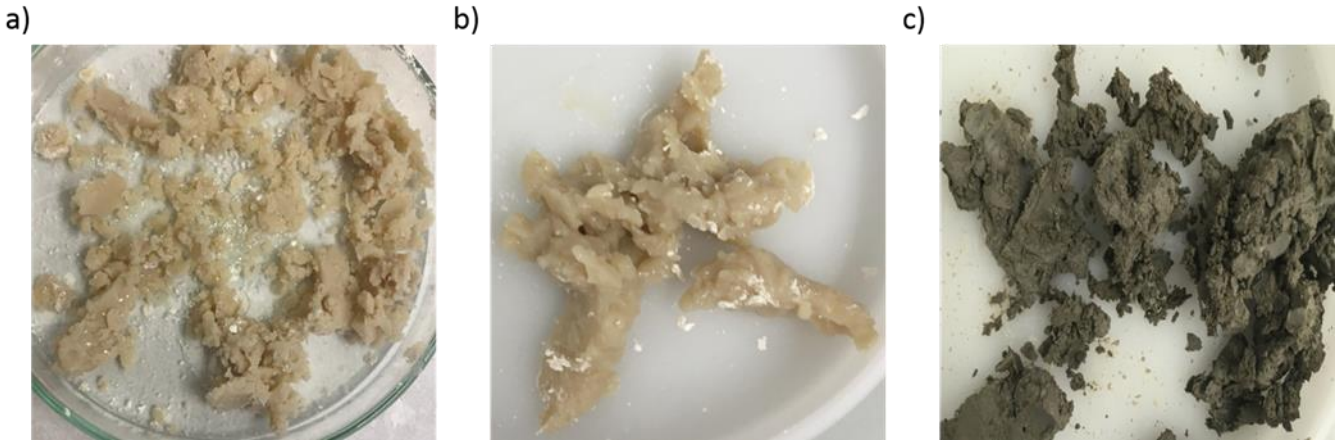

Figure 15 – Appearance of the paste produced with a) alumina and ZIF-8, b) CMC and ZIF-8 and c) alumina and MIL-53(Al).

The second step is the extrusion process. The appearance of the obtained extrudates can be seen in Figure 16. The final extrudates have quite distinct appearances, even when the adsorbent used was the same.

The pastes containing ZIF-8 and CMC, because they were so wet, frequently glued to the screw, thus being necessary to stop the extrusion process several times, to aggregate the paste close to the front of the screw, closer to the dye. Finally, the pastes containing MIL-53(Al) and alumina, although they are not as wet as the ones containing ZIF-8 and alumina, they also glued to the screw. However, with these pastes, it was not necessary to place them close to the die because, after some time, the paste moved closer to the dye. Additionally, some separation between the powder and the water was observed during the extrusion process, and for that reason, it was more challenging to produce pellets without cracks. The drying of the extrudates at room temperature was relatively fast; the difference in color between the dry and wet parts was rapidly observed.

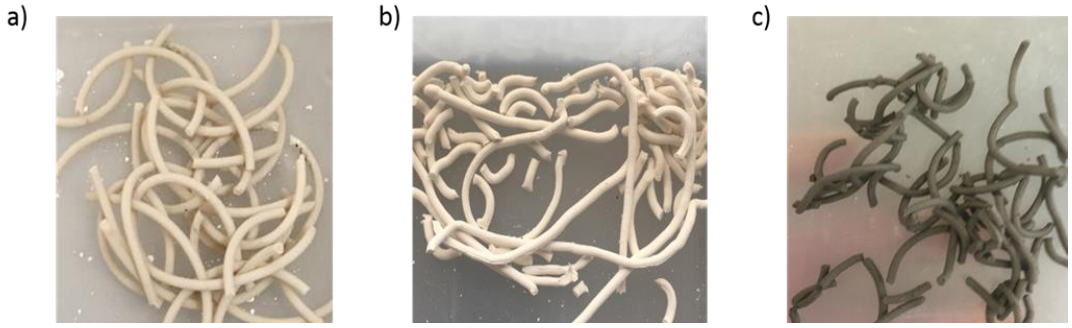

Figure 16 – Extrudates of a) ZIF-8 with alumina as the binder, b) ZIF-8 with CMC as the binder and c) MIL-53(Al) with alumina as the binder.

Lastly, the extrudates were manually cut into pellets. To guarantee that the final material is resistant, a thermal treatment was done to the pellets. The obtained pellets can be observed in Figure 17.

Figure 17 – Pellets of a) ZIF-8-PA5, b) ZIF-8-PA10, c) ZIF-8-15, d) MIL-53(Al)-PA5, e) MIL-53(Al)-PA10, f) MIL-53(Al)-PA15, g) ZIF-8-PC5 and h) ZIF-8-PC10.

4.2.2 Monoliths

It is expected to obtain materials, pellets and monoliths, with good adsorption properties and mechanically resistant. This way, the objective is to produce monoliths with the less quantity of binder possible but resistant. Yet, the inks to produce monoliths must present some flexibility to be easily printed.

The first attempt to print a monolith was made with an ink containing 15 %wt. of alumina and ZIF-8 (see Figure 18 a)) after verifying that the paste seemed to have the rheological properties needed to be printed (*i.e.*, the viscosity decreases with the increase of the shear rate and presents a gel point). However, in the printing step, the system used was not able to extrude the paste loaded into the syringe, even clogging the tube that connects the syringe to the nozzle. This behavior of the ink could be associated with a low homogeneity of the paste even after a long time of mixture. In Figure 18 a) can be observed that the ink has lumps, which may be the reason why the system ZIF-8 + alumina did not work to produce monoliths using a DIW technique. Another possible reason is a fast drying of the paste. Consequently, it was assumed that would not be possible to print the pastes with higher amount of alumina as the binder since they have higher viscosity and a higher gel point than the one with 15 %wt.

a) b) c)

Figure 18 – Appearance of the inks for 3D printing containing a) ZIF-8 + alumina, b) ZIF-8 + CMC and c) MIL-53(Al) + PE + kaolin.

A second attempt to print a monolith was made with the ink having 5 %wt. of CMC and ZIF-8 (see the appearance Figure 18 b)). A monolith was printed with success, but after drying at room temperature, the monolith presented some cracks, see Figure 19. To prevent the formation of cracks another attempt with ink containing 10 %wt. of CMC was done. Once again, a monolith was successfully printed; however, contrary to the expectations, the monolith after drying at room temperature also presented some cracks.

No improvements were verified with the increase in the amount of binder used. Thus, it was inferred that this behavior could be caused by a rapid drying of the paste, not allowing the water to evaporate slowly. This fast drying of the ink could result in a weak aggregation of the adsorbent with the binder. To overcome this situation, the plate was cooled down while the monolith was being printed and during the drying process. Besides this, the environment around the printed monolith was also kept cold. Although the drying process has been slowed down, the monolith presented cracks and broke itself in several parts after some time. The evolution of the monolith along the time can be observed in Figure 20. This way, since a monolith with CMC, has already been printed [100], it was concluded that ZIF-8 + CMC paste are suitable for 3D printing, however do not produce mechanically stable materials.

Finally, the paste containing MIL-53(Al), kaolin, and PE (see Figure 18 c)) was successfully used to print a monolith that is shown in Figure 21. Although the printing step was problematic since the paste was not continuously extruded, a monolith was printed. Figure 21 shows some printing failures that occurred during the printing step. The material produced does not present cracks like the others; however, does not seem to have high mechanical resistance.

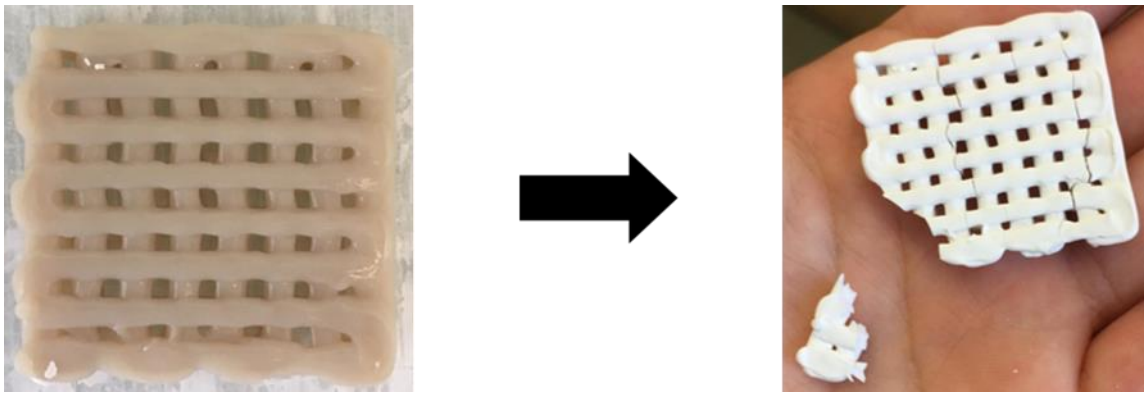

Figure 19 – ZIF-8-MC5 monolith after the printing step.

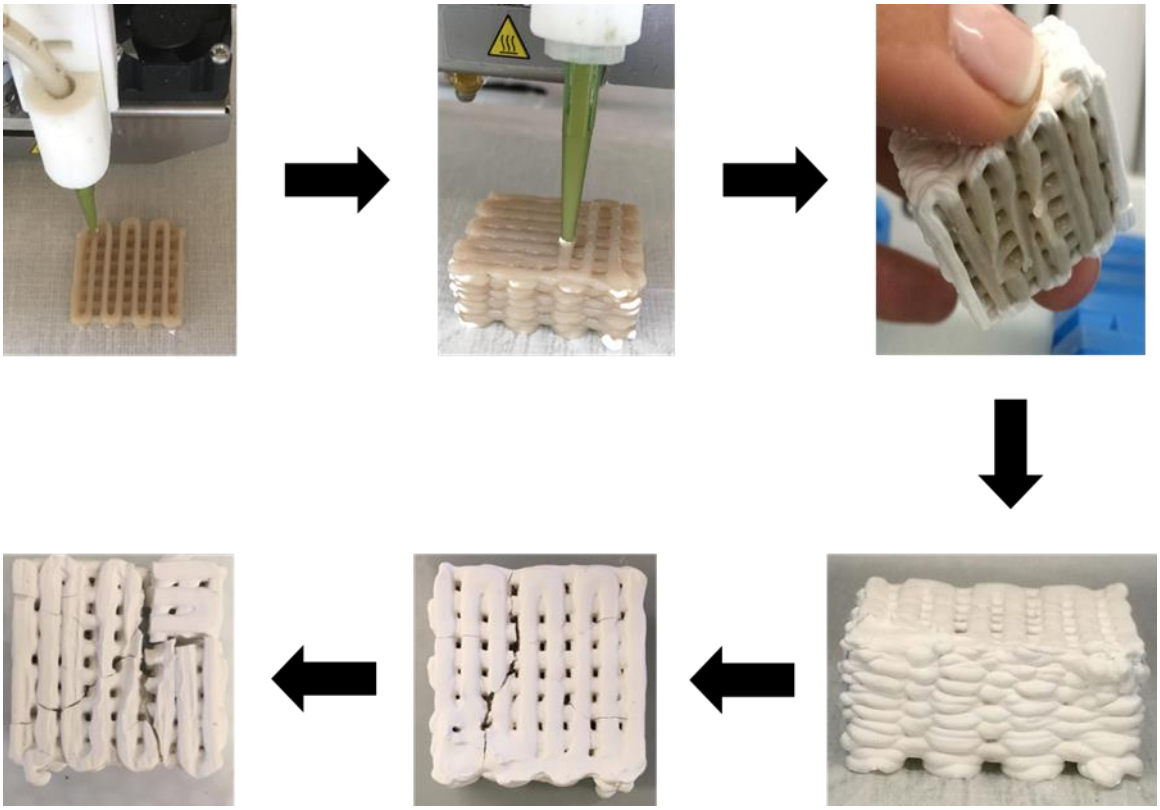

Figure 20 – Evolution of the ZIF-8-MC10.

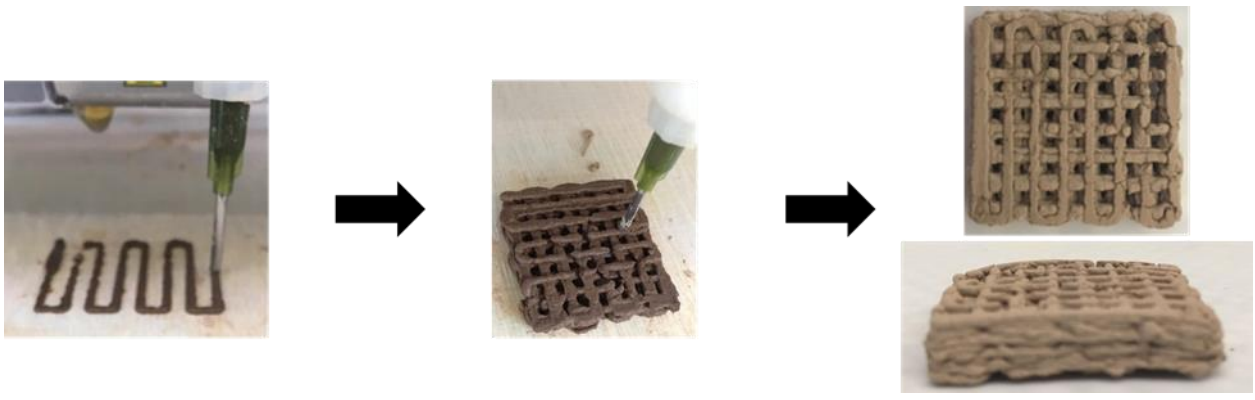

Figure 21 – Evolution of the MIL-53(Al)-M.

Besides that, to guarantee that this shaping process was successful, the printing parameters had to be carefully chosen. The controlled parameters were the printing speed, the infill density, the layer height, and the wall thickness. The printing speed is an essential parameter because if the speed is too high, the details of the monolith may not be well printed. However, it also cannot be too slow because the flow that is coming out of the nozzle becomes more unstable. The layer height must be defined in a way that the layer that is being printed, "glues" to the previous layer of monolith, ensuring that the new layer does not crush the one below. Another critical parameter is related to the thickness of the wall in the horizontal direction. The infill density is associated with the quantity of material that is coming out of the nozzle, the higher the infill density, the higher the amount. The printing parameters used to print the monoliths are summarized in Table 7.

Table 7 - Summary of the defined parameters for 3D printing.

	ZIF-8		MIL-53
	+ 5 %wt. of CMC	+ 10 %wt. of CMC	+ 5 %wt. of PE + 5 %wt. of kaolin
Printing speed ($mm \cdot s^{-1}$)	1.05	0.9-1.05	1.05
Infill density (%)	200-250	250-300	250-300
Layer Height (mm)	0.60	0.60	1.00
Wall Thickness (mm)	0.84	0.84	0.84

To obtain mechanical resistant monoliths with these adsorbents, other combinations of binders should be used in the future.

There are innumerous factors that affect the printing step like the defined printing parameters and the mixing step specifications, like the quantity of solvent used, the mixing velocity, and the mixing time. This way, various combinations of all the parameters that affect the printing step must be studied to produce an optimized monolith. Having into account the deadlines of this work, the values presented previously are the ones that exhibit the best results.

4.3 Characterization

Due to the low mechanical resistance of the MIL-53-(Al) it was decided not to do the characterization tests with this material.

4.3.1 SEM with EDS

The scanning electron microscopy permits to have images from the surface of the samples through the detection of the signal coming from the interaction of the electron beam with the atoms of the samples. In addition to this, with energy-dispersive X-ray spectroscopy, it is possible to analyze the composition of the material. This technique consists in the interaction of the X-rays with the sample that through the measurement of the energy of the X-rays emitted

from the sample creates a spectrum where each peak corresponds to a given element present in the sample.

SEM images for the ZIF-8 powder and the pellets of ZIF-8 containing alumina were obtained and can be observed in Figure 22 and Figure 23, respectively.

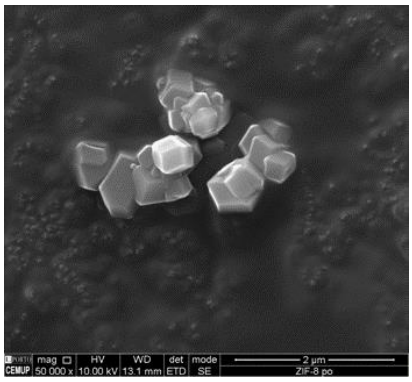

Figure 22 - SEM image of the ZIF-8 crystals.

a)

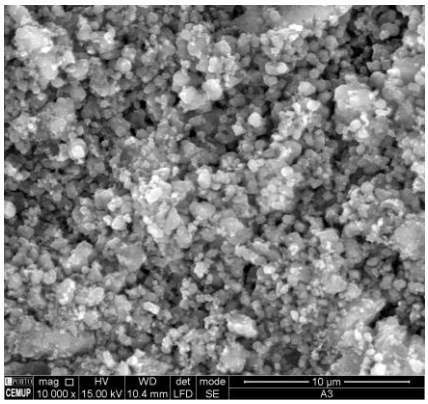

b)

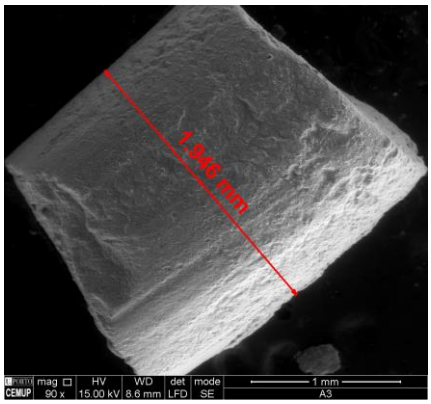

c)

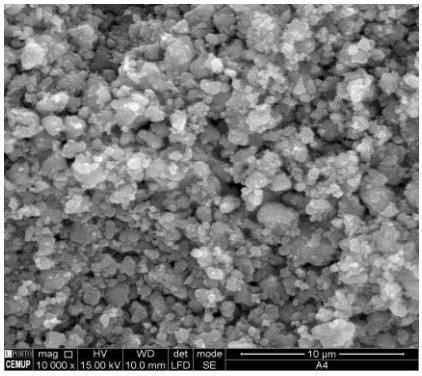

d)

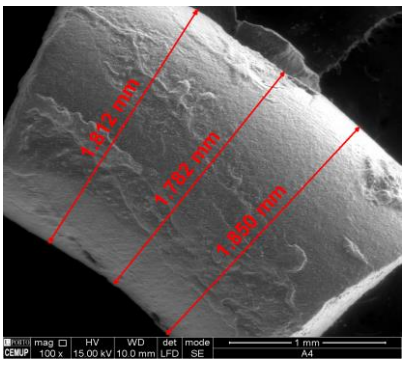

e)

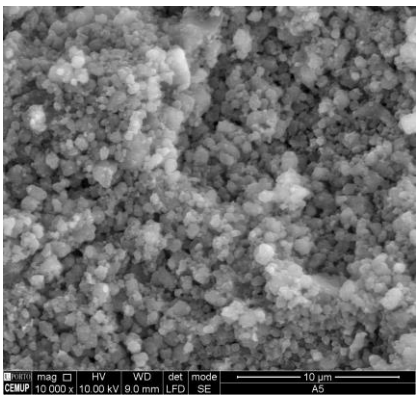

f)

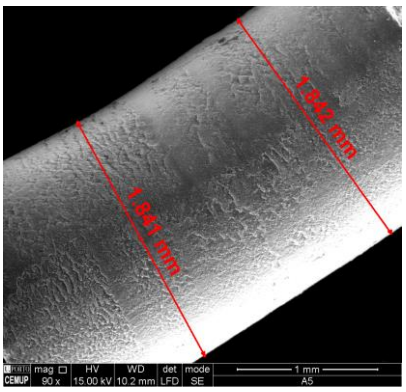

Figure 23 – SEM images of the a) interior of ZIF-8-PA5 with x10 000 magnification, b) pellet of ZIF-8-PA5 with x90 magnification, c) interior of ZIF-8-PA10 with x10 000 magnification, d) pellet of ZIF-8-PA10 with x90 magnification, e) interior of ZIF-8-PA15 with x10 000 magnification, f) pellet of ZIF-8-PA15 with x90 magnification.

In Figure 22, the crystal agglomerates of ZIF-8 with *c.a.* 1.35 μm can be observed. When comparing with pellets samples that contain alumina (see Figure 23), it is possible to verify that there are no distinct zones, proving this way that the mixtures used to produce the pellets were homogeneous. With the increase of the binder amount, no significant alterations could be seen in the surface of the pellets (compare Figure 23 a), c) and e)). Besides that, and as expected, the produced pellets have approximately the same diameter than the orifices of the die (Figure 23 b), d) and f)). The little decrease verified is due to the drying of the pellets and consequent aggregation of the materials present in the pellet.

In addition to this, EDS spectrums were obtained for the ZIF-8 powder and the pellets samples containing alumina. These spectrums can be observed in Figure 24 and Figure 25, respectively.

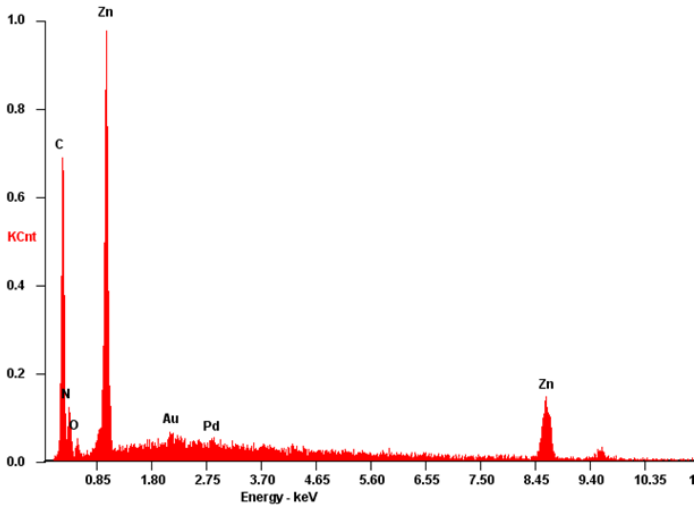

Figure 24 – EDS spretum of ZIF-8 powder.

Seeing Figure 24, six elements can be noted, zinc (Zn), palladium (Pd), gold (Au), oxygen (O), nitrogen (N) and carbon (C). By observation of Figure 3, C, Zn, and N were expected. Having into account the treatment that the samples have suffered before the analyses, it was expected

to find also Au and Pd. However, the element O appeared in the spectrum. This is an impurity of the sample.

For the pellets, as estimated, with the addition of Al_2O_3, an aluminum peak appeared (Figure 25). There is also an increase in the O peak in comparison to the powder form, as expected.

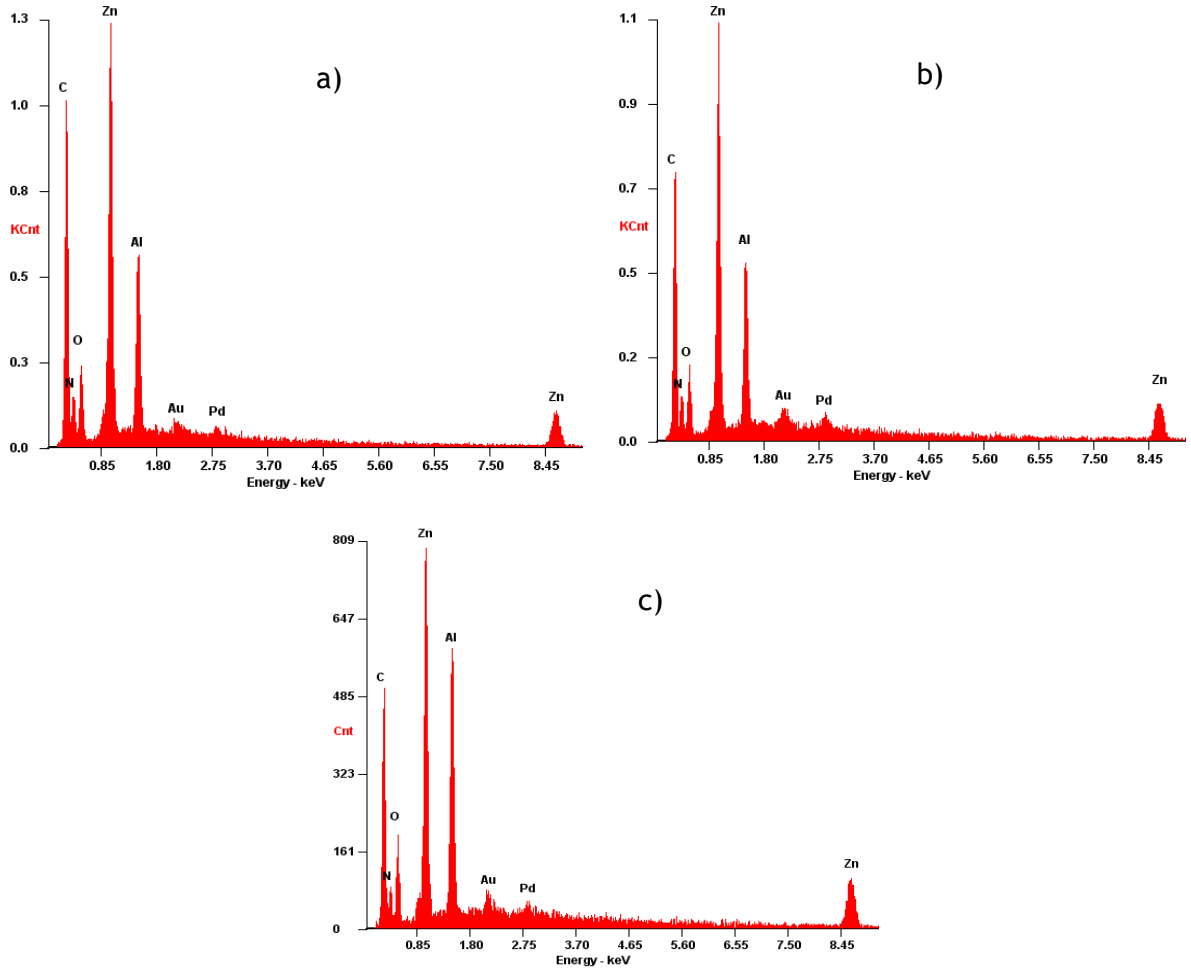

Figure 25 - EDS spectrums of a) ZIF-8-PA5, b) ZIF-8-PA10 and c) ZIF-8-PA15.

4.3.2 XRD

XRD analyses were carried out to understand if the crystalline structure of the adsorbents undergoes some change due to the shaping process. The XRD graphs are presented in Figure 26.

In Figure 26 a) it is possible to observe the XRD patterns for the ZIF-8 samples. When comparing the shaped material with the original powder, it is possible to notice that for all the samples, all characteristic peaks of the ZIF-8 material are kept.

For the samples of MIL-53(Al) (see Figure 26 b)) all the peaks can be observed in the three shaped samples, even though some have higher or lower intensity.

The fact that the peaks presented in the shaped samples are the same than the ones of the correspondent powder means that the crystalline structure remains unchanged with the shaping techniques and with the conditions chosen for the thermal treatment.

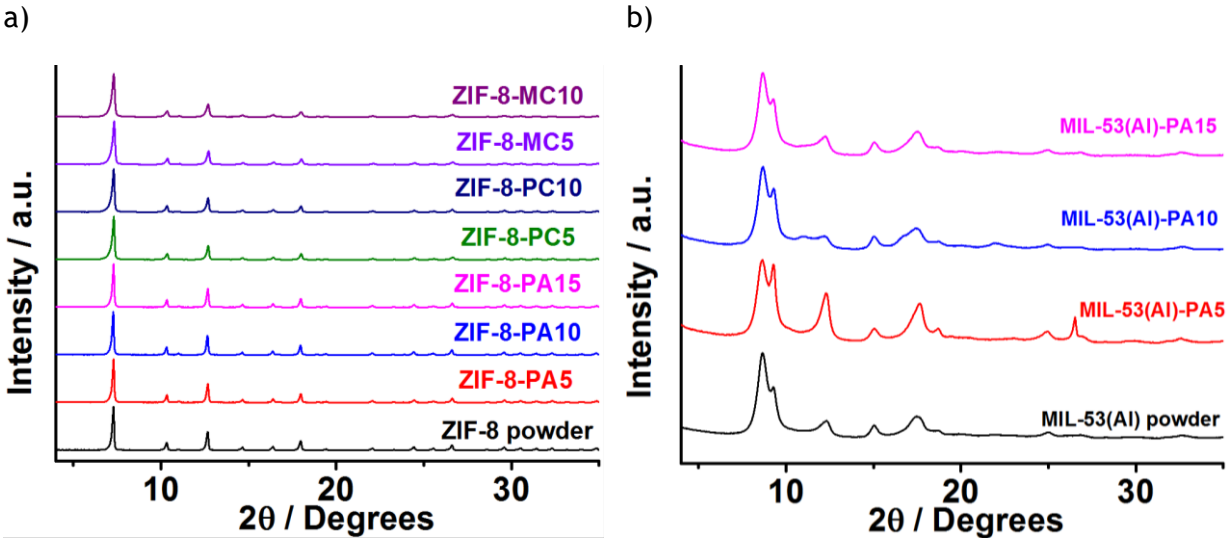

Figure 26 - XRD patterns of the shaped materials of a) ZIF-8, b) MIL-53(Al).

4.3.3 Textural Characterization

4.3.3.1 Mercury Porosimetry

With mercury porosimetry technique it is possible to measure the distribution of meso/macropores of a solid sample and to quantify them. Figure C.1 and Figure C.2 show the cumulative volume of meso/macropores and the differential intrusion as function of pore size diameters for ZIF-8 and MIL-53(Al) materials, respectively. In Table 8 and Table 9, the values of average pore diameter, assuming cylindrical pores, and of apparent density obtained using this technique are summarized for the samples with ZIF-8 and MIL-53(Al), respectively.

Table 8 - Intrusion data summary for shaped materials with ZIF-8.

	ZIF-8						
	-PA5	-PA10	-PA15	-PC5	-PC10	-MC5	-MC10
Average Pore Diameter (nm)	95.8	84.1	62.6	144.7	123.1	114.7	103.7
Apparent density ($g \cdot cm^{-3}$)	0.58	0.62	0.68	0.56	0.60	0.58	0.60

Table 9 - Intrusion data summary for the shaped materials with MIL-53(Al).

	MIL-53(Al)		
	-PA5	-PA10	-PA15
Average Pore Diameter (nm)	33.0	26.7	27.9
Apparent density ($g \cdot cm^{-3}$)	0.67	0.69	0.67

Taking a close look at Table 8 it is possible to observe that, for ZIF-8 materials, using the same shaping technique, the increase of binder content results in a lower average pore diameter, increasing, in this way, the apparent density values. This fact was expected since the function of the binder is to aggregate the material. It is noteworthy that for this microporous adsorbent the value average pore diameter is only related to the interparticle distance. When comparing materials with different type of binders but with the same binder amount and produced by the same shaping technique (extrusion), like ZIF-8-PA5 and ZIF-8-PC5, or ZIF-8-PA10 and ZIF-8-PC10 it is possible to infer that the pellets prepared with alumina have a lower average pore diameter than the ones prepared with CMC. Another aspect that must be highlighted is when using the same adsorbent but different shaping techniques, like with ZIF-8-PC5 and ZIF-8-MC5 or with ZIF-8-PC10 and ZIF-8-MC10, the average pore diameter is lower when using 3D printing, producing this way a more aggregated material.

For the MIL-53(Al) pellets the addition of binder does not seem to have a significant impact on the values obtained (see Table 9). However, it was expected that for MIL-53(Al)-PA15 the value of the average pore diameter was lower, and the apparent density value was higher than the ones presented for MIL-53(Al)-PA10 for the reasons mentioned previously. Probably, this difference can have interference in the obtained values. The difference is possibly related to the excessive use of solvent in the shaping process.

4.3.3.2 N_2 adsorption at 77 K and CO_2 adsorption at 273 K

N_2 adsorption measurements at 77 K were performed to determine the surface area and the micropore volume of the samples. The values determined for ZIF-8 and MIL-53(Al) materials are reported in Table 10 and Table 11, respectively.

The pore volume for pores lower than 7.97 Å can be obtained by CO_2 adsorption at 273 K. These values for the ZIF-8 and MIL-53(Al) materials are presented in Table 10 and Table 11, respectively.

Table 10 – Summary of the data of N_2 adsorption at 77 K and CO_2 adsorption at 273 K for ZIF-8 materials.

	ZIF-8							
	Powder	-PA5	-PA10	-PA15	-PC5	-PC10	-MC5	-MC10
Langmuir surface area ($m^2 \cdot g^{-1}$)	1970	1673	1677	1522	1723	1689	1665	1576
Micropore volume ($cm^3 \cdot g^{-1}$)	0.69	0.58	0.58	0.53	0.61	0.59	0.58	0.55
Pore volume (< 7.97 Å) ($cm^3 \cdot g^{-1}$)	0.065	0.055	0.057	0.053	0.057	0.056	0.057	0.055

Table 11 - Summary of the data of N_2 adsorption at 77 K and CO_2 adsorption at 273 K for MIL-53(Al) materials.

	MIL-53(Al)			
	Powder	PA5	PA10	PA15
Langmuir surface area ($m^2 \cdot g^{-1}$)	853	722	667	682
Micropore volume ($cm^3 \cdot g^{-1}$)	0.25	0.21	0.19	0.19
Pore volume (< 7.97 Å) ($cm^3 \cdot g^{-1}$)	0.15	0.13	0.12	0.12

It would be expected that for the materials with the same components an increase in the binder amount would result in a decrease in the Langmuir surface area and in the micropore volume. That is verified for all the materials with exception of ZIF-8-PA5 and ZIF-8-PA10, which present, approximately, the same values for these parameters.

For ZIF-8 materials, it is verified that the one that presented a lower decrease in the parameters was the ZIF-8-PC5 (see Table 10). Further investigation on adsorption properties and on the mechanical strength of this material (ZIF-8-PC5) must be carried out in the future.

In the open literature, a study of the variation of the surface area of extrudates of Basolite® Z1200 with different amounts of PVA as binder was performed [112]. It is observed that for lower amounts of binder, the loss of surface area in relation to the pristine powder is approximately equal to the amount used to prepare the extrudates. With the increase of the amount of binder used, this value becomes bigger than the amount of the binder used, evidencing pore blockage. In this work, for the ZIF-8 pellets, for the lowest amount of binder used a pore blockage is already observed, since the value of loss surface area in relation to the commercial powder is superior to the amount of binder used.

For the MIL-53(Al) materials the decreasing on all the parameters with the increase of the binder amount is verified. For these materials when comparing the values of micropore volume with the pore volume (<7.97 Å) it is observed that the percentage of the micropores with diameter lower than 7.97 Å is higher when compared to the ZIF-8 materials. The adsorption isotherms of N_2 at 77 K and CO_2 at 273 K for ZIF-8 and MIL-53(Al) materials can be observed in the Appendix D.

4.4 Mechanical Strength Tests

Maximum crushing strength tests were performed only for pellet samples containing alumina - see Figure 27.

As expected, for ZIF-8 pellets, the higher the amount of the binder, the higher the maximum crushing strength, *i.e*, the higher must be the force applied on the pellet to crush it (Figure 27). For the ZIF-8 pellets, the higher value obtained was for the ZIF-8-PA15 pellets (9.5 N).

Considering a value of 2 mm for the pellet diameter, the ZIF-8-PA15 pellets have a mechanical strength value of 4.75 $N \cdot mm^{-1}$.

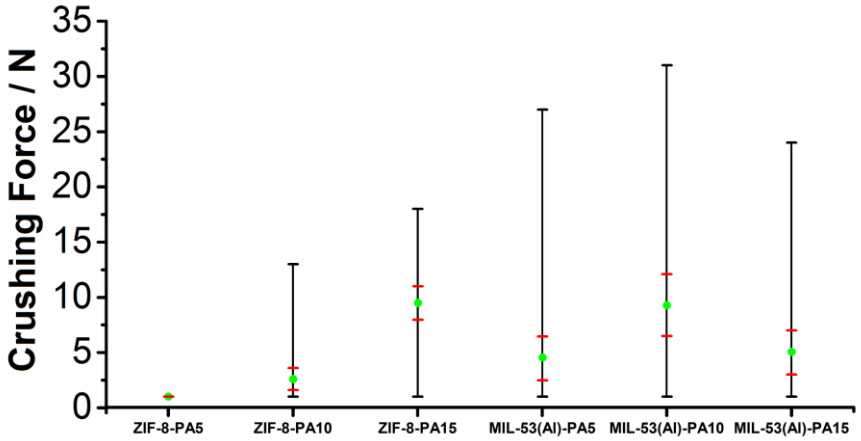

Figure 27 - Overview of the maximum crushing strength; (green) average maximum crushing strength, (red) 95 % confidence interval of the average, (black) range of the maximum crushing strengths.

However, for the MIL-53(Al) pellets it is not verified the same behavior - Figure 27. The pellets prepared with 10 %wt. of alumina have higher maximum crushing strength than the ones that contain 15 %wt. of alumina (9.3 N vs 5 N). Once again this can be attributed to a possible excessive use of water in the preparation of MIL-53(Al)-PA15 pellets. For the MIL-53(Al)-PA10 pellets, considering the pellet diameter already mentioned, a value mechanical strength of 4.65 $N \cdot mm^{-1}$ was obtained.

Comparing this results with the ones of mercury porosimetry (Table 8 and Table 9), it is possible to observe that the maximum crushing strength results are possibly related with the average pore diameters values: for the same adsorbent, the lower the interparticular distances, the higher the maximum crushing strength values.

In the open literature, crushing force tests were performed on a shaped ZIF-8 tablet with 5 %wt. of mothocel binder prepared by dry pressing technique. A value of 6.5 $N \cdot mm^{-1}$ was obtained for the mechanical strength of the material [113]. Even though the shaping technique used is not the same as the presented in this work to prepare these materials, the crushing force of the pellets ZIF-8 and 15 %wt. of alumina and of the MIL-53(Al)-PA10 is in good agreement with ones reported in the literature.

Some improvements can still be made in relation to the mechanical strength of the materials, and for that, some other binders or mixtures of binders must be studied. Nevertheless, ZIF-8-PA15 and MIL-53(Al)-PA10 already present a significant mechanical strength to be used, at least in a laboratory scale.

4.5 Adsorption Equilibrium Isotherms

In a preliminary phase, without previously knowing the results of textural characterization and of the crushing force tests, the pellets that in theory would have better properties of adsorption would be ZIF-8-PA5 and MIL-53(Al)-PA5, since they possess less amount of binder. Therefore, they were chosen to perform adsorption equilibrium isotherms measurements for CH_4 and N_2, for pressure values up to 4 bar, at 303 K. The Langmuir adsorption model was used to fit the experimental data - Equation 4. The isotherm parameters for the both shaped material for CH_4 and N_2 were determined by minimization of the sum of the quadratic differences between the experimental points and the value of the quantity adsorbed calculated by the Langmuir fitting. The minimization was performed employing the Excel Solver add-in.

$$q = q_{\mathrm{m}} \frac{bP}{1 + bP} \qquad \text{Equation 4}$$

In Equation 4, q is the quantity adsorbed, q_{m} is the maximum adsorption capacity, b is the adsorption equilibrium constant and P is the pressure.

Figure 28 and Figure 29 presents the isotherms obtained for CH_4 for the both shaped materials and for the pristine powders. In Table 12 the Langmuir isotherm parameters for CH_4 and N_2 on ZIF-8-PA5 and MIL-53(Al)-PA5 are reported.

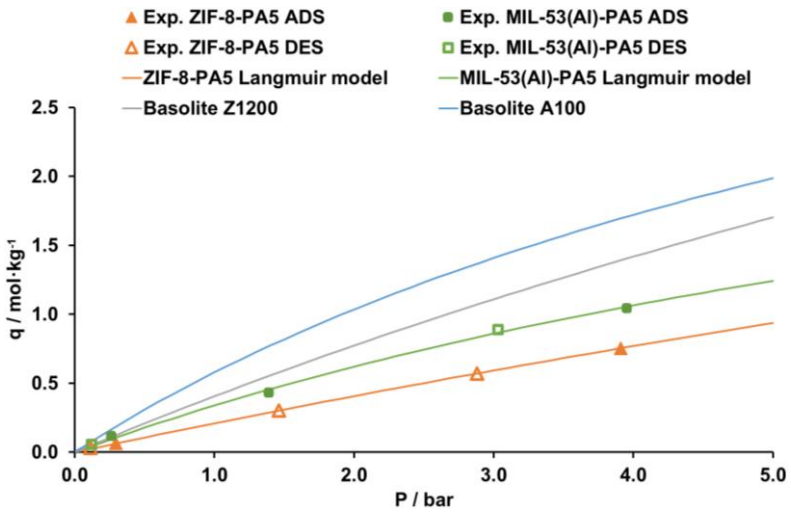

Figure 28 - CH_4 adsorption equilibrium isotherms measurements on ZIF-8-PA5 pellets at 303 K (orange triangles - closed adsorption, open desorption; orange line - Langmuir model) and on MIL-53(Al)-PA5 pellets at 303 K (green squares - closed adsorption, open desorption; green line- Langmuir model). On open literature: Basolite A100 at 303 K (blue line) from [103] and Basolite Z1200 at 298 K (grey line) [114].

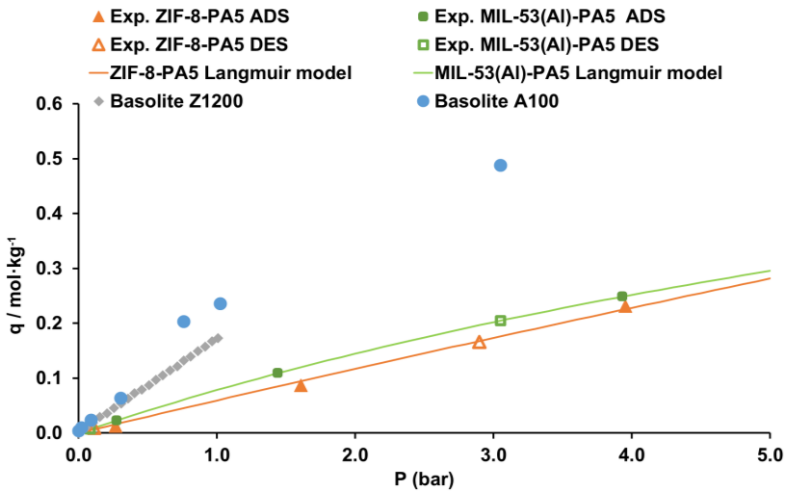

Figure 29 - N_2 adsorption equilibrium isotherms measurements on ZIF-8-PA5 pellets at 303 K (orange triangles - closed adsorption, open desorption; orange line - Langmuir model) and on MIL-53(Al)-PA5 pellets at 303 K (green squares - closed adsorption, open desorption; green line - Langmuir model). On open literature: Basolite A100 at 303 K (blue circles) from [115] and Basolite Z1200 at 298 K (grey diamonds) from [116].

For the both gases tested, for pressures up to 4 bar, the capacities of adsorption of the MIL-53(Al)-PA5 are higher than the ones of ZIF-8-PA5 – Figure 28 and Figure 29. Besides this, the Langmuir adsorption model represents a good fit of the experimental adsorption points.

Table 12 - Langmuir isotherm parameters for CH_4 and N_2 on ZIF-8-PA5 and MIL-53(Al)-PA5.

	ZIF-8-PA5		MIL-53(Al)-PA5	
	CH_4	N_2	CH_4	N_2
q_m (mol·kg^{-1})	7.16	4.46	3.74	0.97
b (bar^{-1})	3.01 x 10^{-2}	1.35 x 10^{-2}	9.94 x 10^{-2}	8.77 x 10^{-2}

For the separation of CH_4 and N_2 it is essential to understand the variation of the selectivity (Equation 6) with the total pressure. Since the Langmuir adsorption model is a good fit of the experimental values and considering a stream with a molar fraction of 0.6 of CH_4 and 0.4 of N_2, the selectivity as function of pressure can be represented – Figure 30.

$$\alpha_{i,j} = \frac{q_i}{x_i}\frac{x_j}{q_j} \qquad \text{Equation 5}$$

In Equation 5, $\alpha_{i,j}$ is the selectivity between the component i and j, x_i is the molar fraction of the component i, and x_j is the molar fraction of the component j.

For all the range of pressures MIL-53(Al)-PA5 presents a higher selectivity for the CH_4 than ZIF-8-PA5 - Figure 30. Therefore, for CH_4/N_2 separations for pressures up to 6 bar the use of MIL-53 shaped material is preferable. It is noteworthy that no further assumptions for higher pressures should be made, because the experimental data is for partial pressures up to 4 bar, and for that reason the model can only be used to fit this data and not extrapolate the values for higher pressures.

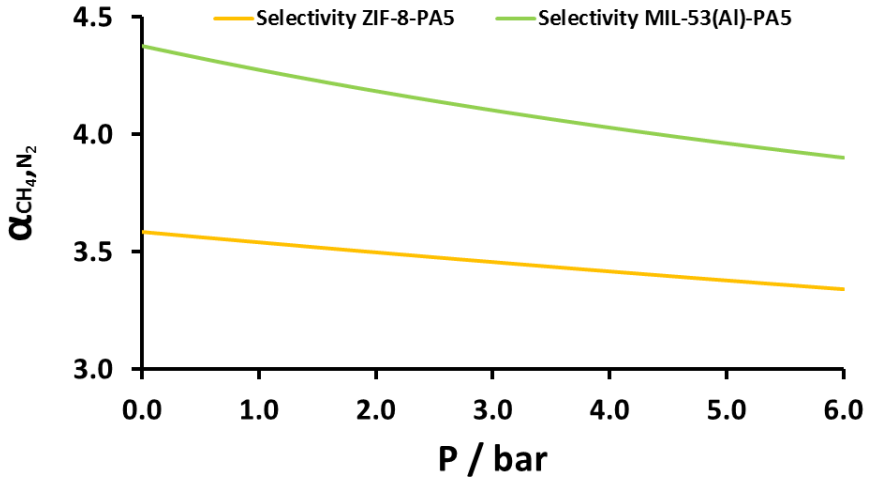

Figure 30 - Selectivity as function of the total pressure. ZIF-8-PA5 (orange line); MIL-53(Al)-PA5 (green line).

Table 13 - Summary of the values of the loss adsorption capacity at 1 bar in the shaped materials.

	ZIF-8-PA5		MIL-53(Al)-PA5	
	CH_4	N_2	CH_4	N_2
Loss of adsorption capacity (%)	< 48.43	< 65.77	41.50	66.75

Since the adsorption capacity of the commercial powder (Basolite Z1200) was measured at 298 K and the adsorption phenomena is an exothermic process, lower values of adsorption capacities were expected at 303 K, and for that is the reason why the values of loss of adsorption capacity reported in Table 13 are lower than 48.43 and 65.77 % (not a fixed values).

For both materials it is verified that the effects of shaping are more significant for N_2 than for CH_4. However, to understand the effect of the shaping on the adsorption capacities of the shaped materials, a study related to the loss capacity as function of the pressure should be done. To do this study, it would be necessary to determine the adsorption equilibrium isotherms of the both gases for the ZIF-8 and MIL-53(Al) commercials powders at 303 K.

5 Conclusions

To ensure a good performance of the adsorbents on an industrial scale, these materials must be shaped in order to grant a good mass and thermal transference, a low pressure drop and a great mechanical stability. In this way, in this work the shaping of ZIF-8 and MIL-53(Al) powders into pellets and monoliths, using alumina, CMC, kaolin and PE as binders was studied. Two techniques were employed in this process: extrusion and 3D printing.

Rheological tests were performed on the inks containing the adsorbent and the binders to ensure that it has the correct properties to be printed, like the pseudoplastic behavior. All the inks tested presented a pseudoplastic behavior.

With the purpose of understand the effect of the quantity of binder, the type of binder and the shaping technique on the final properties of the prepared material, a chemical and morphological characterization was performed. For both adsorbents, it is verified that the shaping process and the thermal treatment has no impact on the crystalline structure of the adsorbents. In general, with the increase of the amount of binder, when the adsorbent and the shaping technique used are the same, the final material presents a lower average pore diameter (interparticular space) and a lower surface area. This last one it is especially critical since for the same adsorbent, lower the surface area, lower the capacity of the material to adsorb. Besides this, the crushing tests allowed to comprehend that for the ZIF-8-PA pellets, the higher the amount of the alumina, the higher the force that must be exerted to crush the pellet. For the MIL-53(Al) pellets the same did not occur, however, it is thought that the reason for this to happen is related with the excessive use of solvent in the shaping process.

Finally, measurements of adsorption equilibrium isotherms for CH_4 and N_2 at 303 K using ZIF-8-PA5 and MIL-53(Al)-PA5 for pressure values up to 4 bar were performed. The Langmuir adsorption model has proven to be able to fit the experimental results. For both adsorbents the adsorption capacity of the material for CH_4 is higher than the one for N_2. Considering the values of selectivity for the both adsorbents tested, it is verified that for the range of pressure the use of MIL-53 adsorbent, due to its higher selectivity, is preferable for CH_4/N_2 separations.

5.1 Achieved Objectives

The first objective of this work was to shape ZIF-8 and MIL-53(Al) powder adsorbents into pellets and monoliths by employing extrusion and 3D printing techniques. Pellets for the both adsorbents were obtained with success. It was also possible to print the monoliths employing both materials.

Adsorption equilibrium isotherms for CH_4 and N_2 on ZIF-8-PA5 and MIL-53(Al)-PA5 were measured. The Langmuir adsorption model was able to fit the experimental data. MIL-53(Al)-PA5 showed higher selectivity than ZIF-8-PA5 for the CH_4/N_2 separation.

5.2 Limitations and Future Work

All the characterization tests, crushing force tests, and adsorption equilibrium measurements should be performed for all the shaped samples, to have a better understanding of which is the best adsorbent produced. However, given the available time it was not feasible to do this. Therefore, characterization tests should be performed in all the shaped materials to completely understand the behavior of the materials.

For future work other binders must be studied to ensure a significant mechanical strength of the materials and to test if there are other binders that have a minor impact in the adsorption properties of the material. For the monoliths it is necessary to find a binder that ensures that there is no cracks formation and that the prepared material is mechanically resistant. Combinations of various binders to prepare the ink for 3D printing must be tried because there are binders that provide viscosity to the ink and other binders that provide flexibility.

Besides this, the adsorption equilibrium isotherms for the commercial powders at 303 K must be measured to comprehend the effect of the shaping on the selectivity of the materials. With these isotherms it would be interesting to do a study of variation of the loss adsorption capacity with the pressure.

5.3 Final Assessment

The assessment of this work is positive once the main objectives were accomplished. Yet, there are some improvements that can be made to the shaped materials.

This work was a pleasant challenge that allowed me to test my acquired skills during these five years.

6 References

1. Yang, R.T., *Gas Separation by Adsorption Processes*, ed. R.T. Yang. 1987: Butterworth-Heinemann. 1-8.
2. Li, J.-R., R.J. Kuppler, and H.-C. Zhou, *Selective gas adsorption and separation in metal-organic frameworks.* Chemical Society Reviews, 2009. **38**(5): p. 1477-1504.
3. Akhtar, F., L. Andersson, S. Ogunwumi, N. Hedin, and L. Bergström, *Structuring adsorbents and catalysts by processing of porous powders.* Journal of the European Ceramic Society, 2014. **34**(7): p. 1643-1666.
4. Kida, K., M. Okita, K. Fujita, S. Tanaka, and Y. Miyake, *Formation of high crystalline ZIF-8 in an aqueous solution.* CrystEngComm, 2013. **15**(9): p. 1794-1801.
5. Tomic, E.A., *Thermal stability of coordination polymers.* Journal of Applied Polymer Science, 1965. **9**(11): p. 3745-3752.
6. Mueller, U., M. Schubert, F. Teich, H. Puetter, K. Schierle-Arndt, and J. Pastré, *Metal-organic frameworks—prospective industrial applications.* Journal of Materials Chemistry, 2006. **16**(7): p. 626-636.
7. Min Wang, Q., D. Shen, M. Bülow, M. Ling Lau, S. Deng, F.R. Fitch, N.O. Lemcoff, and J. Semanscin, *Metallo-organic molecular sieve for gas separation and purification.* Microporous and Mesoporous Materials, 2002. **55**(2): p. 217-230.
8. Samsonenko , D.G., H. Kim, Y. Sun, G.-H. Kim, H.-S. Lee, and K. Kim, *Microporous Magnesium and Manganese Formates for Acetylene Storage and Separation.* Chemistry – An Asian Journal, 2007. **2**(4): p. 484-488.
9. Lin, X., A.J. Blake, C. Wilson, X.Z. Sun, N.R. Champness, M.W. George, P. Hubberstey, R. Mokaya, and M. Schröder, *A Porous Framework Polymer Based on a Zinc(II) 4,4'-Bipyridine-2,6,2',6'-tetracarboxylate: Synthesis, Structure, and "Zeolite-Like" Behaviors.* Journal of the American Chemical Society, 2006. **128**(33): p. 10745-10753.
10. Borjigin, T., F. Sun, J. Zhang, K. Cai, H. Ren, and G. Zhu, *A microporous metal-organic framework with high stability for GC separation of alcohols from water.* Chem Commun (Camb), 2012. **48**(61): p. 7613-5.
11. Zhou, W., H. Wu, M.R. Hartman, and T. Yildirim, *Hydrogen and Methane Adsorption in Metal−Organic Frameworks: A High-Pressure Volumetric Study.* The Journal of Physical Chemistry C, 2007. **111**(44): p. 16131-16137.
12. Eddaoudi, M., J. Kim, N. Rosi, D. Vodak, J. Wachter, M. O'Keeffe, and O.M. Yaghi, *Systematic Design of Pore Size and Functionality in Isoreticular MOFs and Their Application in Methane Storage.* Science, 2002. **295**(5554): p. 469-472.
13. Liu, C., F. Sun, S. Zhou, Y. Tian, and G. Zhu, *Facile synthesis of ZIF-8 nanocrystals in eutectic mixture.* CrystEngComm, 2012. **14**(24): p. 8365-8367.
14. Eddaoudi, M., J. Kim, N. Rosi, D. Vodak, J. Wachter, M. Keeffe, and O.M. Yaghi, *Systematic Design of Pore Size and Functionality in Isoreticular MOFs and Their Application in Methane Storage.* Science, 2002. **295**(5554): p. 469.
15. Britt, D., D. Tranchemontagne, and O.M. Yaghi, *Metal-organic frameworks with high capacity and selectivity for harmful gases.* Proceedings of the National Academy of Sciences, 2008. **105**(33): p. 11623-11627.
16. Liu, Y., V.C. Kravtsov, R. Larsen, and M. Eddaoudi, *Molecular building blocks approach to the assembly of zeolite-like metal-organic frameworks (ZMOFs) with extra-large cavities.* Chemical Communications, 2006(14): p. 1488-1490.
17. Pan, L., D.H. Olson, L.R. Ciemnolonski, R. Heddy, and J. Li, *Separation of Hydrocarbons with a Microporous Metal-Organic Framework.* Angewandte Chemie International Edition, 2006. **45**(4): p. 616-619.

18. Koh, K., A.G. Wong-Foy, and A.J. Matzger, *A Porous Coordination Copolymer with over 5000 m2/g BET Surface Area.* Journal of the American Chemical Society, 2009. **131**(12): p. 4184-4185.

19. D'Alessandro, D.M., B. Smit, and J.R. Long, *Carbon Dioxide Capture: Prospects for New Materials.* Angewandte Chemie International Edition, 2010. **49**(35): p. 6058-6082.

20. Férey, G., *Hybrid porous solids: past, present, future.* Chemical Society Reviews, 2008. **37**(1): p. 191-214.

21. Loiseau, T., C. Serre, C. Huguenard, G. Fink, F. Taulelle, M. Henry, T. Bataille, and G. Ferey, *A rationale for the large breathing of the porous aluminum terephthalate (MIL-53) upon hydration.* Chemistry, 2004. **10**(6): p. 1373-82.

22. Greathouse, J.A. and M.D. Allendorf, *The Interaction of Water with MOF-5 Simulated by Molecular Dynamics.* Journal of the American Chemical Society, 2006. **128**(33): p. 10678-10679.

23. Schröck, K., F. Schröder, M. Heyden, R.A. Fischer, and M. Havenith, *Characterization of interfacial water in MOF-5 (Zn4(O)(BDC)3)—a combined spectroscopic and theoretical study.* Physical Chemistry Chemical Physics, 2008. **10**(32): p. 4732-4739.

24. Park, K.S., Z. Ni, A.P. Cote, J.Y. Choi, R. Huang, F.J. Uribe-Romo, H.K. Chae, M. O'Keeffe, and O.M. Yaghi, *Exceptional chemical and thermal stability of zeolitic imidazolate frameworks.* Proc Natl Acad Sci U S A, 2006. **103**(27): p. 10186-10191.

25. Miller, S.R., P.A. Wright, T. Devic, C. Serre, G. Férey, P.L. Llewellyn, R. Denoyel, L. Gaberova, and Y. Filinchuk, *Single Crystal X-ray Diffraction Studies of Carbon Dioxide and Fuel-Related Gases Adsorbed on the Small Pore Scandium Terephthalate Metal Organic Framework, Sc2(O2CC6H4CO2)3.* Langmuir, 2009. **25**(6): p. 3618-3626.

26. Chowdhury, P., C. Bikkina, D. Meister, F. Dreisbach, and S. Gumma, *Comparison of adsorption isotherms on Cu-BTC metal organic frameworks synthesized from different routes.* Microporous and Mesoporous Materials, 2009. **117**(1): p. 406-413.

27. Fletcher, A.J., K.M. Thomas, and M.J. Rosseinsky, *Flexibility in metal-organic framework materials: Impact on sorption properties.* Journal of Solid State Chemistry, 2005. **178**(8): p. 2491-2510.

28. Dincă, M. and J.R. Long, *Strong H2 Binding and Selective Gas Adsorption within the Microporous Coordination Solid Mg3(O2C-C10H6-CO2)3.* Journal of the American Chemical Society, 2005. **127**(26): p. 9376-9377.

29. Férey, G., M. Latroche, C. Serre, F. Millange, T. Loiseau, and A. Percheron-Guégan, *Hydrogen adsorption in the nanoporous metal-benzenedicarboxylate M(OH)(O2C–C6H4–CO2) (M = Al3+, Cr3+), MIL-53.* Chemical Communications, 2003(24): p. 2976-2977.

30. Ferreira, A.F.P., A.M. Ribeiro, S. Kulaç, and A.E. Rodrigues, *Methane purification by adsorptive processes on MIL-53(Al).* Chemical Engineering Science, 2015. **124**: p. 79-95.

31. Kim, P.-J., Y.-W. You, H. Park, J.-S. Chang, Y.-S. Bae, C.-H. Lee, and J.-K. Suh, *Separation of SF6 from SF6/N2 mixture using metal-organic framework MIL-100(Fe) granule.* Chemical Engineering Journal, 2015. **262**.

32. Institute, E.P.R., *Program on Technology Innovation: Post-combustion CO2 Capture Technology Development.* 2008.

33. Banerjee, R., H. Furukawa, D. Britt, C. Knobler, M. O'Keeffe, and O.M. Yaghi, *Control of Pore Size and Functionality in Isoreticular Zeolitic Imidazolate Frameworks and their Carbon Dioxide Selective Capture Properties.* Journal of the American Chemical Society, 2009. **131**(11): p. 3875-3877.

34. García, H. and S. Navalón, *Metal-Organic Frameworks: Applications in Separations and Catalysis*. 2018: John Wiley & Sons.

35. Wang, B., A.P. Côté, H. Furukawa, M. O'Keeffe, and O.M. Yaghi, *Colossal cages in zeolitic imidazolate frameworks as selective carbon dioxide reservoirs.* Nature, 2008. **453**(7192): p. 207.

36. Banerjee, R., A. Phan, B. Wang, C. Knobler, H. Furukawa, M. O'Keeffe, and O.M. Yaghi, *High-throughput synthesis of zeolitic imidazolate frameworks and application to CO2 capture.* Science, 2008. **319**(5865): p. 939-43.

37. Hayashi, H., A.P. Cote, H. Furukawa, M. O'Keeffe, and O.M. Yaghi, *Zeolite A imidazolate frameworks.* Nature materials, 2007. **6**(7): p. 501.

38. Li, Y., F. Liang, H. Bux, W. Yang, and J. Caro, *Zeolitic imidazolate framework ZIF-7 based molecular sieve membrane for hydrogen separation.* Journal of Membrane Science, 2010. **354**(1): p. 48-54.
39. Cousin-Saint-Remi, J., A.-L. Finoulst, C. Jabbour, G.V. Baron, and J.F.M. Denayer, *Selection of binder recipes for the formulation of MOFs into resistant pellets for molecular separations by fixed-bed adsorption.* Microporous and Mesoporous Materials, 2019.
40. Inanc, I. and O. Yazaydin, *Screening of Zeolitic Imidazolate Frameworks for Preconcentration of Hazardous Chemicals*, in *Nanotechnology to Aid Chemical and Biological Defense*. 2015, Springer. p. 177-189.
41. Hughes, J.T., D.F. Sava, T.M. Nenoff, and A. Navrotsky, *Thermochemical Evidence for Strong Iodine Chemisorption by ZIF-8.* Journal of the American Chemical Society, 2013. **135**(44): p. 16256-16259.
42. Peralta, D., G. Chaplais, A. Simon-Masseron, K. Barthelet, and G.D. Pirngruber, *Separation of C6 Paraffins Using Zeolitic Imidazolate Frameworks: Comparison with Zeolite 5A.* Industrial & Engineering Chemistry Research, 2012. **51**(12): p. 4692-4702.
43. Böhme, U., B. Barth, C. Paula, A. Kuhnt, W. Schwieger, A. Mundstock, J. Caro, and M. Hartmann, *Ethene/Ethane and Propene/Propane Separation via the Olefin and Paraffin Selective Metal–Organic Framework Adsorbents CPO-27 and ZIF-8.* Langmuir, 2013. **29**(27): p. 8592-8600.
44. Martins, V.F., A.M. Ribeiro, P. Kortunov, A. Ferreira, and A.E. Rodrigues, *High purity ethane/ethylene separation by gas phase simulated moving bed using ZIF-8 adsorbent.* AIChE Journal.
45. Ferreira, A.F., M.C. Mittelmeijer-Hazeleger, M.A. Granato, V.F.D. Martins, A.E. Rodrigues, and G. Rothenberg, *Sieving di-branched from mono-branched and linear alkanes using ZIF-8: experimental proof and theoretical explanation.* Physical Chemistry Chemical Physics, 2013. **15**(22): p. 8795-8804.
46. Rezaei, F. and P. Webley, *Optimum structured adsorbents for gas separation processes.* Chemical Engineering Science, 2009. **64**(24): p. 5182-5191.
47. Flank, W.H., W.P. Fethke Jr, and J. Marte, *Process for preparing molecular sieve bodies*. 1989, Google Patents.
48. Howell, P.A. and N.A. Acara, *Process for producing molecular sieve bodies*. 1964, Google Patents.
49. Yang, K., Q. Sun, F. Xue, and D. Lin, *Adsorption of volatile organic compounds by metal-organic frameworks MIL-101: Influence of molecular size and shape.* Journal of Hazardous Materials, 2011. **195**: p. 124-131.
50. Golden, C.M.A., T.C. Golden, and P.J. Battavio, *Multilayered adsorbent system for gas separations by pressure swing adsorption*. 2005, Google Patents.
51. Keefer, B.G. and C.R. McLean, *High frequency rotary pressure swing adsorption apparatus*. 2000, Google Patents.
52. Yanase, I., Y. Yamakawa, and H. Kobayashi, *CO₂ absorption of CaO coated on aluminosilicate foam.* Journal of the Ceramic Society of Japan, 2008. **116**(1350): p. 176-180.
53. Andersson, L., F. Akhtar, A. Ojuva, and L. Bergström, *Colloidal processing and CO2-capture performance of hierarchically porous Al2O3-zeolite 13X composites.* Journal of Ceramic Science and Technology, 2012. **3**(1): p. 9-16.
54. Jaffe, S.M. and C.I. Contescu, *Adsorbent sheet material for parallel passage contactors*. 2006, Google Patents.
55. Lively, R., R.R. Chance, W.J. Koros, H.W. Deckman, and B.T. Kelley, *Sorbent fiber compositions and methods of temperature swing adsorption.* 2013.
56. Leta, D.P., H.W. Deckman, P.I. Ravikovitch, and B.A. DeRites, *Rapid temperature swing adsorption contactors for gas separation*. 2014, Google Patents.
57. Patil, M.D. and J.L. Williams, *Temperature actuated zeolite in-line adsorber system*. 1996, Google Patents.
58. Bolz, F., *Advanced materials in catalysis*. 2013: Elsevier.
59. Keshavarzi, N., *Structuring porous adsorbents and composites for gas separation and odor removal*. 2014, Department of Materials and Environmental Chemistry (MMK), Stockholm University.

60. Ren, J., H.W. Langmi, B. North, and M. Mathe, *Review on processing of metal-organic framework (MOF) materials towards system integration for hydrogen storage*. International Journal of Energy Research, 2014. **39**.

61. Akhtar, F. and L. Bergström, *Colloidal Processing and Thermal Treatment of Binderless Hierarchically Porous Zeolite 13X Monoliths for CO2 Capture*. Journal of the American Ceramic Society, 2011. **94**(1): p. 92-98.

62. Bae, J.M., S. Ahmed, R. Kumar, and E. Doss, *Microchennel development for autothermal reforming of hydrocarbon fuels*. Journal of Power Sources, 2005. **139**(1): p. 91-95.

63. Wang, H., L. Huang, Z. Wang, A. Mitra, and Y. Yan, *Hierarchical zeolite structures with designed shape by gel-casting of colloidal nanocrystal suspensions*. Chemical Communications, 2001(15): p. 1364-1365.

64. Twiname, E.R. and R.E. Mistler, *Tape Casting and Lamination*, in *Encyclopedia of Materials: Science and Technology*, K.H.J. Buschow, et al., Editors. 2001, Elsevier: Oxford. p. 9083-9088.

65. Restuccia, G., A. Freni, and G. Maggio, *A zeolite-coated bed for air conditioning adsorption systems: parametric study of heat and mass transfer by dynamic simulation*. Applied Thermal Engineering, 2002. **22**(6): p. 619-630.

66. Farhan binti Azha, S., S. Abd Hamid, and S. Ismail, *Development of Composite Adsorbent Coating Based Acrylic Polymer/Bentonite for Methylene Blue Removal*. Journal of Engineering and Technological Sciences, 2017. **49**: p. 225-235.

67. Valdés-Solís, T., M.J.G. Linders, F. Kapteijn, G. Marbán, and A.B. Fuertes, *Adsorption and breakthrough performance of carbon-coated ceramic monoliths at low concentration of n-butane*. Chemical Engineering Science, 2004. **59**(13): p. 2791-2800.

68. Öhrman, O., J. Hedlund, and J. Sterte, *Synthesis and evaluation of ZSM-5 films on cordierite monoliths*. Applied Catalysis A: General, 2004. **270**(1): p. 193-199.

69. Hutmacher, D.W., T.B.F. Woodfield, and P.D. Dalton, *Chapter 10 - Scaffold Design and Fabrication*, in *Tissue Engineering (Second Edition)*, C.A.V. Blitterswijk and J. De Boer, Editors. 2014, Academic Press: Oxford. p. 311-346.

70. Dehghani, F. and N. Annabi, *Engineering porous scaffolds using gas-based techniques*. Current Opinion in Biotechnology, 2011. **22**(5): p. 661-666.

71. Patel, R., M. Patel, and A. Suthar, *Spray drying technology: an overview*. Indian Journal of Science and Technology, 2009. **2**(10): p. 44-47.

72. Ren, J. and B.C. North, *Shaping porous materials for hydrogen storage applications: a review*. Journal of Technology Innovations in Renewable Energy, 2014. **3**(1): p. 12-20.

73. Vasiliev, P., F. Akhtar, J. Grins, J. Mouzon, C. Andersson, J. Hedlund, and L. Bergström, *Strong Hierarchically Porous Monoliths by Pulsed Current Processing of Zeolite Powder Assemblies*. ACS Applied Materials & Interfaces, 2010. **2**(3): p. 732-737.

74. Hamzah, H.H., S.A. Shafiee, A. Abdalla, and B.A. Patel, *3D printable conductive materials for the fabrication of electrochemical sensors: A mini review*. Electrochemistry Communications, 2018. **96**: p. 27-31.

75. Feilden, E., *Additive manufacturing of ceramics and ceramic composites via robocasting*. 2017.

76. Hull, C.W., *Apparatus for production of three-dimensional objects by stereolithography*. 1986, Google Patents.

77. Robinson, E. and W.M.T.M. Reimerink-Schats, *Composite adsorbent material*. 2014, Google Patents.

78. Serrano, D.P., R. Sanz, P. Pizarro, I. Moreno, P. de Frutos, and S. Blázquez, *Preparation of extruded catalysts based on TS-1 zeolite for their application in propylene epoxidation*. Catalysis Today, 2009. **143**(1): p. 151-157.

79. Young, D.A. and G.A. Mickelson, *Alumina-bonded catalysts*. 1971, Google Patents.

80. Whiting, G.T., A.D. Chowdhury, R. Oord, P. Paalanen, and B.M. Weckhuysen, *The curious case of zeolite-clay/binder interactions and their consequences for catalyst preparation*. Faraday Discussions, 2016. **188**(0): p. 369-386.

81. Dorado, F., R. Romero, and P. Cañizares, *Hydroisomerization of n-butane over Pd/HZSM-5 and Pd/Hβ with and without binder*. Applied Catalysis A: General, 2002. **236**(1): p. 235-243.

82. Dorado, F., R. Romero, and P. Cañizares, *Influence of Clay Binders on the Performance of Pd/HZSM-5 Catalysts for the Hydroisomerization of n-Butane*. Industrial & Engineering Chemistry Research, 2001. **40**(16): p. 3428-3434.

83. Ugal, J.R., M. Mustafa, and A.A. Abdulhadi, *Preparation of zeolite type 13x from locally available raw materials*. Iraqi Journal of Chemical and Petroleum Engineering, 2008. **9**(1): p. 51-56.

84. Golovko, G.A., B.A. Lipkind, A.T. Slepneva, A.S. Leontiev, V.M. Mazin, E.N. Berezovskaya, V.A. Burylov, A.M. Zubkov, O.A. Konakova, and A.I. Judaev, *Process for the preparation of synthetic zeolites*. 1976, Google Patents.

85. Mitchell, W.J. and W.F. Moore, *Bonded molecular sieves*. 1961, Google Patents.

86. Bazer-Bachi, D., B. Harbuzaru, and E. Lecolier, *Mof formed by extrusion and pelletizing with a hydraulic binder having improved mechanical properties and process for preparing same*. 2015, Google Patents.

87. Finsy, V., L. Ma, L. Alaerts, D.E. De Vos, G.V. Baron, and J.F.M. Denayer, *Separation of CO2/CH4 mixtures with the MIL-53(Al) metal-organic framework*. Microporous and Mesoporous Materials, 2009. **120**(3): p. 221-227.

88. Zheng, J., X. Cui, Q. Yang, Q. Ren, Y. Yang, and H. Xing, *Shaping of ultrahigh-loading MOF pellet with a strongly anti-tearing binder for gas separation and storage*. Chemical Engineering Journal, 2018. **354**: p. 1075-1082.

89. Cavenati, S., C.A. Grande, A.E. Rodrigues, C. Kiener, and U. Müller, *Metal Organic Framework Adsorbent for Biogas Upgrading*. Industrial & Engineering Chemistry Research, 2008. **47**(16): p. 6333-6335.

90. Kim, J., S.-H. Kim, S.-T. Yang, and W.-S. Ahn, *Bench-scale preparation of Cu3(BTC)2 by ethanol reflux: Synthesis optimization and adsorption/catalytic applications*. Microporous and Mesoporous Materials, 2012. **161**: p. 48-55.

91. Ren, J., N.M. Musyoka, H.W. Langmi, A. Swartbooi, B.C. North, and M. Mathe, *A more efficient way to shape metal-organic framework (MOF) powder materials for hydrogen storage applications*. International Journal of Hydrogen Energy, 2015. **40**(13): p. 4617-4622.

92. Couck, S., J. Lefevere, S. Mullens, L. Protasova, V. Meynen, G. Desmet, G.V. Baron, and J.F.M. Denayer, *CO2, CH4 and N2 separation with a 3DFD-printed ZSM-5 monolith*. Chemical Engineering Journal, 2017. **308**: p. 719-726.

93. Lefevere, J., L. Protasova, S. Mullens, and V. Meynen, *3D-printing of hierarchical porous ZSM-5: The importance of the binder system*. Materials & Design, 2017. **134**: p. 331-341.

94. Li, X., F. Rezaei, and A.A. Rownaghi, *Methanol-to-olefin conversion on 3D-printed ZSM-5 monolith catalysts: Effects of metal doping, mesoporosity and acid strength*. Microporous and Mesoporous Materials, 2019. **276**: p. 1-12.

95. Thakkar, H., S. Eastman, Q. Al-Naddaf, A. Asghar Rownaghi, and F. Rezaei, *3D-Printed Metal-Organic Framework Monoliths for Gas Adsorption Processes*. ACS Applied Materials & Interfaces, 2017. **9**.

96. Thakkar, H., S. Eastman, A. Hajari, A.A. Rownaghi, J.C. Knox, and F. Rezaei, *3D-Printed Zeolite Monoliths for CO2 Removal from Enclosed Environments*. ACS Applied Materials & Interfaces, 2016. **8**(41): p. 27753-27761.

97. Thakkar, H., S. Eastman, A. Al-Mamoori, A. Hajari, A.A. Rownaghi, and F. Rezaei, *Formulation of Aminosilica Adsorbents into 3D-Printed Monoliths and Evaluation of Their CO2 Capture Performance*. ACS Applied Materials & Interfaces, 2017. **9**(8): p. 7489-7498.

98. Couck, S., J. Cousin-Saint-Remi, S. Van der Perre, G.V. Baron, C. Minas, P. Ruch, and J.F.M. Denayer, *3D-printed SAPO-34 monoliths for gas separation*. Microporous and Mesoporous Materials, 2018. **255**: p. 185-191.

99. Li, X., W. Li, F. Rezaei, and A. Rownaghi, *Catalytic cracking of n-hexane for producing light olefins on 3D-printed monoliths of MFI and FAU zeolites*. Chemical Engineering Journal, 2018. **333**: p. 545-553.

100. Regufe, M.J., A.F.P. Ferreira, J.M. Loureiro, A. Rodrigues, and A.M. Ribeiro, *Electrical conductive 3D-printed monolith adsorbent for CO2 capture*. Microporous and Mesoporous Materials, 2019. **278**: p. 403-413.

101. Loiseau, T., C. Serre, C. Huguenard, G. Fink, F. Taulelle, M. Henry, T. Bataille, and G. Férey, *A Rationale for the Large Breathing of the Porous Aluminum Terephthalate (MIL-53) Upon Hydration*. Chemistry – A European Journal, 2004. **10**(6): p. 1373-1382.

102. Serra-Crespo, P., E. Gobechiya, E.V. Ramos-Fernandez, J. Juan-Alcañiz, A. Martinez-Joaristi, E. Stavitski, C.E.A. Kirschhock, J.A. Martens, F. Kapteijn, and J. Gascon, *Interplay of Metal Node and Amine Functionality in NH2-MIL-53: Modulating Breathing Behavior through Intra-framework Interactions*. Langmuir, 2012. **28**(35): p. 12916-12922.

103. Heymans, N., S. Vaesen, and G. De Weireld, *A complete procedure for acidic gas separation by adsorption on MIL-53 (Al)*. Microporous and Mesoporous Materials, 2012. **154**: p. 93-99.

104. Bourrelly, S., P.L. Llewellyn, C. Serre, F. Millange, T. Loiseau, and G. Férey, *Different Adsorption Behaviors of Methane and Carbon Dioxide in the Isotypic Nanoporous Metal Terephthalates MIL-53 and MIL-47*. Journal of the American Chemical Society, 2005. **127**(39): p. 13519-13521.

105. Low, J.J., A.I. Benin, P. Jakubczak, J.F. Abrahamian, S.A. Faheem, and R.R. Willis, *Virtual High Throughput Screening Confirmed Experimentally: Porous Coordination Polymer Hydration*. Journal of the American Chemical Society, 2009. **131**(43): p. 15834-15842.

106. Dubey, S., A. Dhar Dwivedi, M. Sillanpää, H. Lee, Y.-N. Kwon, and C. Lee, *Adsorption of As(V) by boehmite and alumina of different morphologies prepared under hydrothermal conditions*. Chemosphere, 2017. **169**.

107. Feilden, E., E.G.-T. Blanca, F. Giuliani, E. Saiz, and L. Vandeperre, *Robocasting of structural ceramic parts with hydrogel inks*. Journal of the European Ceramic Society, 2016. **36**(10): p. 2525-2533.

108. Rao, M.A., *Rheology of fluid and semisolid foods: principles and applications*. 2010: Springer Science & Business Media.

109. Lam, C., P.J. Martin, and S.A. Jefferis, *Rheological properties of PHPA polymer support fluids*. Journal of Materials in Civil Engineering, 2015. **27**(11): p. 04015021.

110. Rudolph, N. and T.A. Osswald, *Polymer rheology: fundamentals and applications*. 2014: Carl Hanser Verlag GmbH Co KG.

111. Mezger, T.G., *The rheology handbook: for users of rotational and oscillatory rheometers*. 2006: Vincentz Network GmbH & Co KG.

112. Delgado, J.A., V.I. Águeda, M.A. Uguina, P. Brea, and C.A. Grande, *Comparison and evaluation of agglomerated MOFs in biohydrogen purification by means of pressure swing adsorption (PSA)*. Chemical Engineering Journal, 2017. **326**: p. 117-129.

113. Bazer-Bachi, D., L. Assié, V. Lecocq, B. Harbuzaru, and V. Falk, *Towards industrial use of metal-organic framework: Impact of shaping on the MOF properties*. Powder Technology, 2014. **255**: p. 52-59.

114. Autie-Castro, G., E. Jardim, E. Reguera, E. Vilarrasa-García, E. Rodriguez-Castellon, and C. Cavalcante Jr, *CH4 AND CO2 ADSORPTION STUDY IN ZIF-8 AND AL-BDC MOFS*. 2015.

115. Camacho, B.C.R., R.P.P.L. Ribeiro, I.A.A.C. Esteves, and J.P.B. Mota, *Adsorption equilibrium of carbon dioxide and nitrogen on the MIL-53(Al) metal organic framework*. Separation and Purification Technology, 2015. **141**: p. 150-159.

116. Huang, H., W. Zhang, D. Liu, B. Liu, G. Chen, and C. Zhong, *Effect of temperature on gas adsorption and separation in ZIF-8: A combined experimental and molecular simulation study*. Chemical Engineering Science, 2011. **66**(23): p. 6297-6305.

Appendix A – Helium pycnometries

Assuming that helium is not adsorbed, three helium pycnometry experiments were performed, one where the system was constituted by the basket, the permanent magnet, the glass wool, and the suspension shaft (Figure A.1) and the others constituted by the same things plus the ZIF-8-PA5 and MIL-53-(Al)-PA5 – Figure A.2 a) and b), respectively.

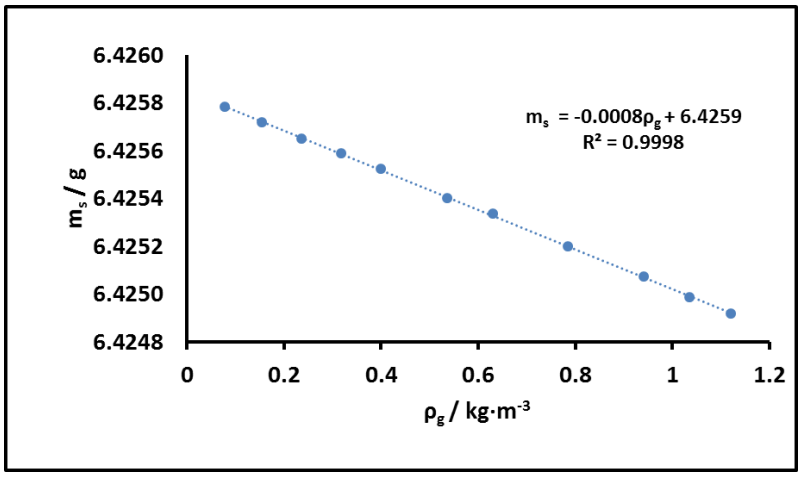

Figure A.1 – Helium pycnometry of system with the basket, the permanent magnet, the glass wool, and the suspension shaft.

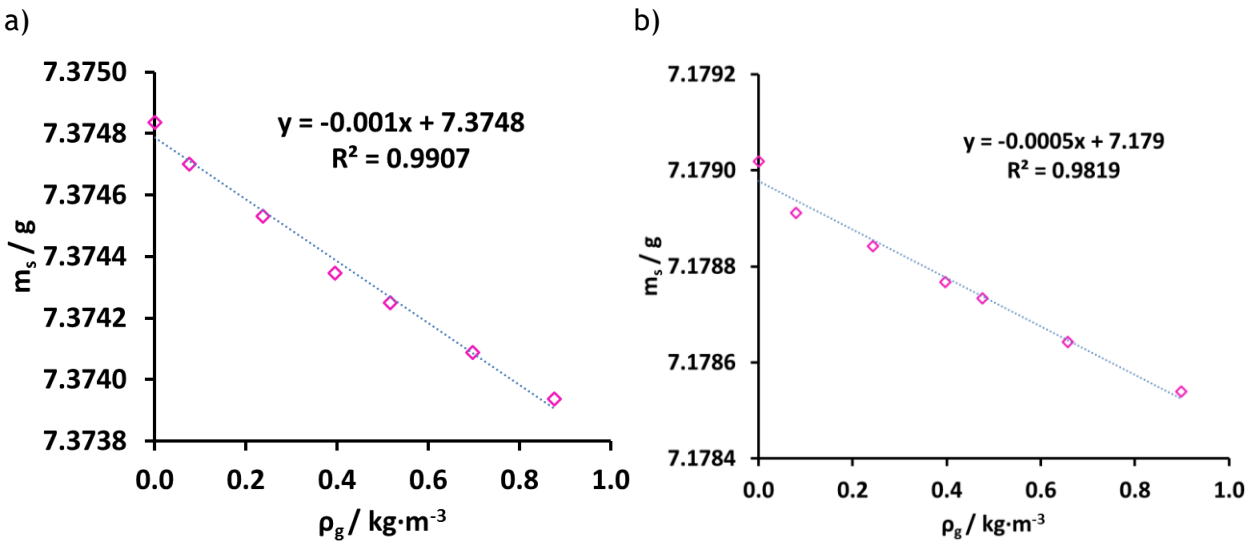

Figure A.2 - Helium pycnometry of system with the basket, the permanent magnet, the glass wool, the suspension shaft and a) ZIF-8-PA5 and b) MIL-53(Al)-PA5.

Appendix B – Rheological behavior results

Figure B.1 and Figure B.2 show the fit of the mathematical models to the experimental results for the pastes with ZIF-8 and the paste containing MIL-53, respectively.

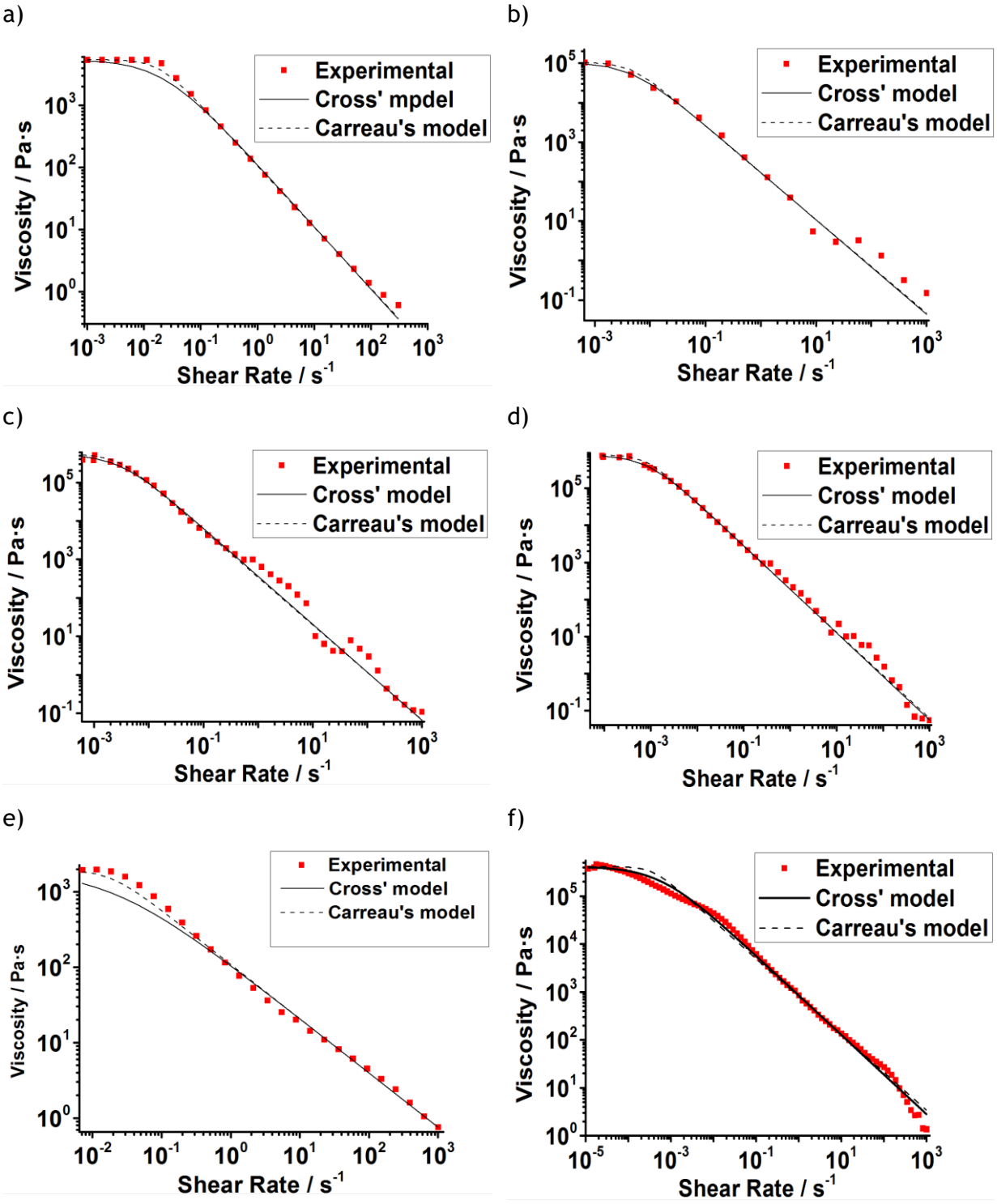

Figure B.1 - Experimental results of viscosity points obtained and the mathematical model that describes the behaviour of the ink containing ZIF-8 and a) 15 %wt of alumina, b) 35 %wt of alumina, c) 50 %wt of alumina, d) 75 %wt of alumina, e) 5 %wt of CMC and f) 10 %wt of CMC.

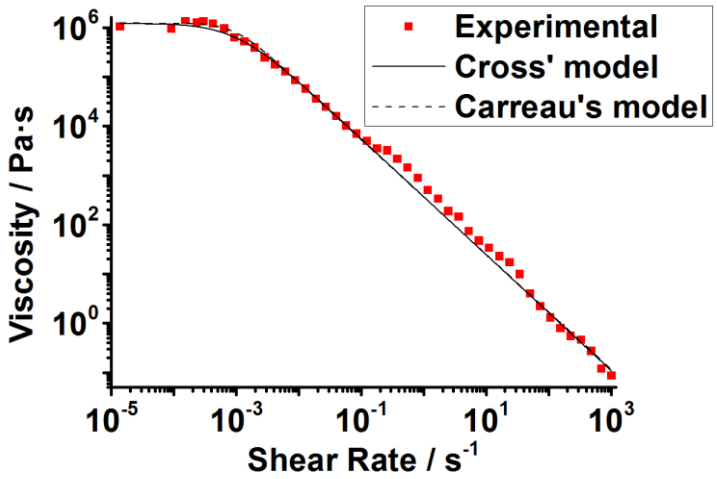

Figure B.2 - Experimental results of viscosity obtained and the mathematical model that describes the behavior of the ink containing MIL-53.

As it can be seen the two mathematical models represent well the experimental data at low and high shear rates.

Appendix C – Mercury porosimetry

Figure C.1 and Figure C.2 show the cumulative volume of meso/macropores and the differential intrusion as function of pore size diameters for ZIF-8 and MIL-53(Al) materials, respectively.

a)

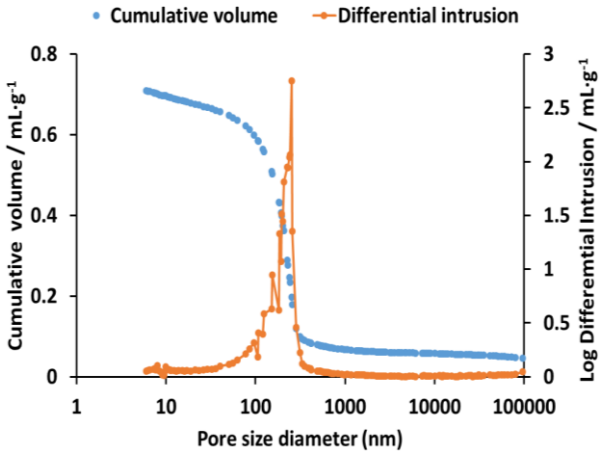

b)

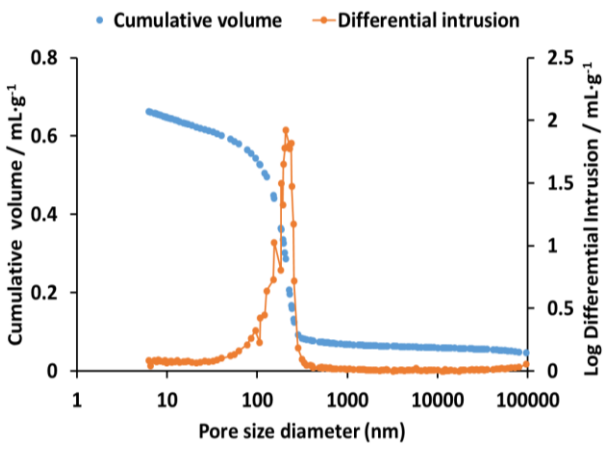

c)

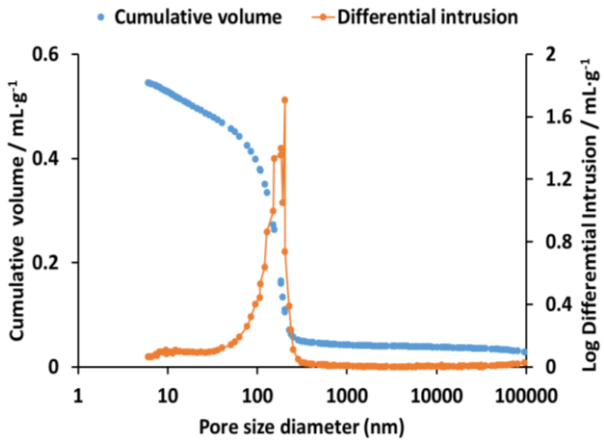

d)

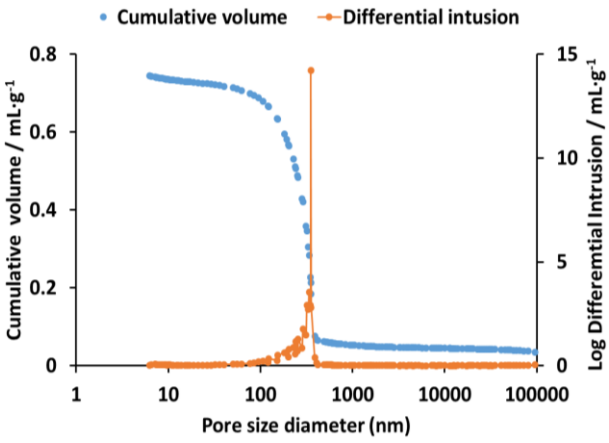

e)

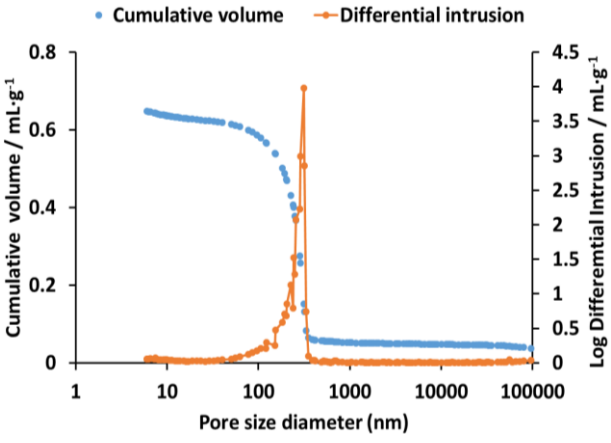

f)

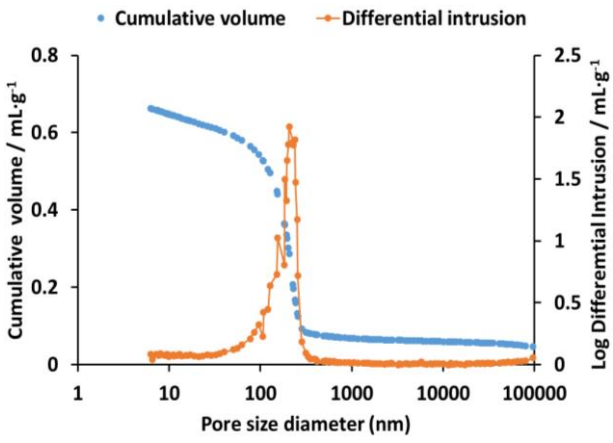

g)

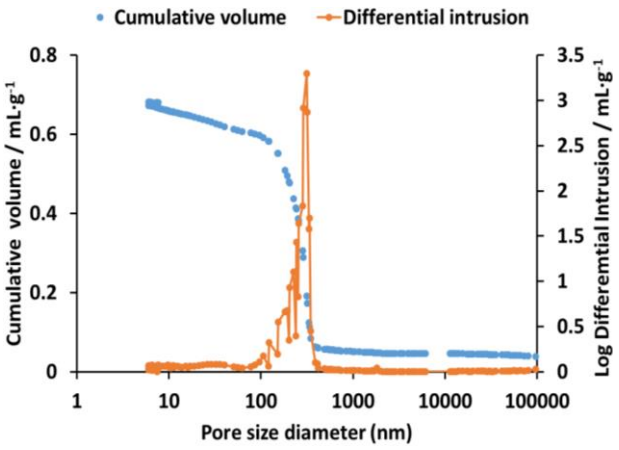

Figure C.1 – Cumulative volume (blue circles) and differential intrusion of Hg intrusive in the meso/macropores (orange circle) of a) ZIF-8-PA5, b) ZIF-8-PA10, c) ZIF-8-PA15, d) ZIF-8-PC5, e) ZIF-8-PC10, f) ZIF-8-MC5 and g) ZIF-8-MC10.

a)

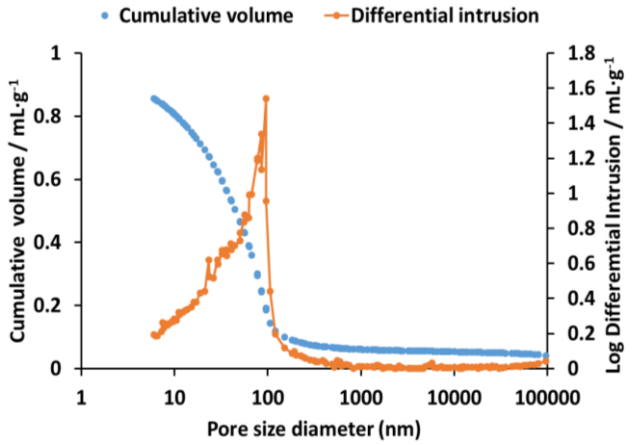

b)

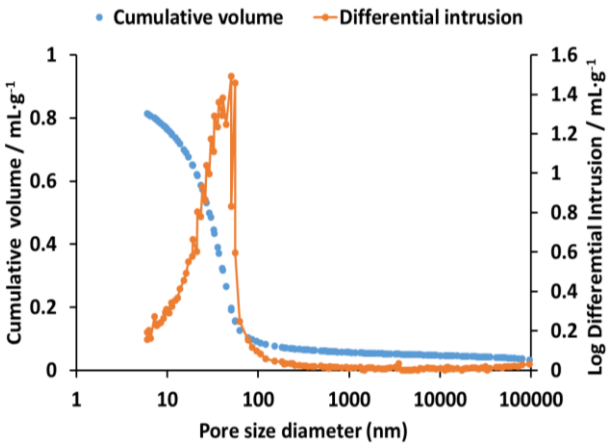

c)

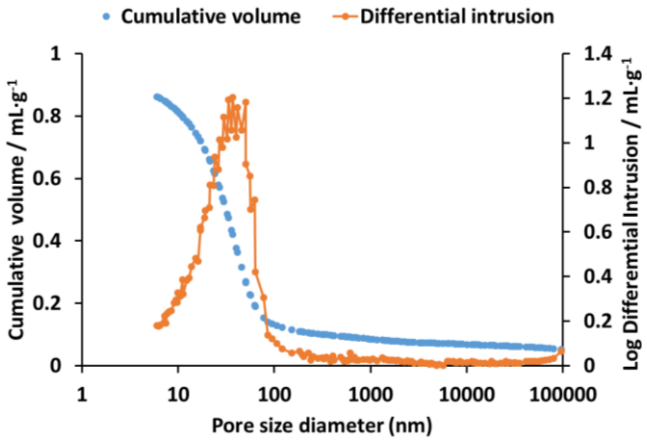

Figure C.2 – Cumulative volume (blue circles) and differential intrusion of Hg intrusive in the meso/macropores (orange circle) of a) MIL-53(Al)-PA5, b) MIL-53(Al)-PA10 and c) MIL-53(Al)-PA15.

Appendix D - N_2 adsorption at 77 K and CO_2 adsorption at 273 K

a)

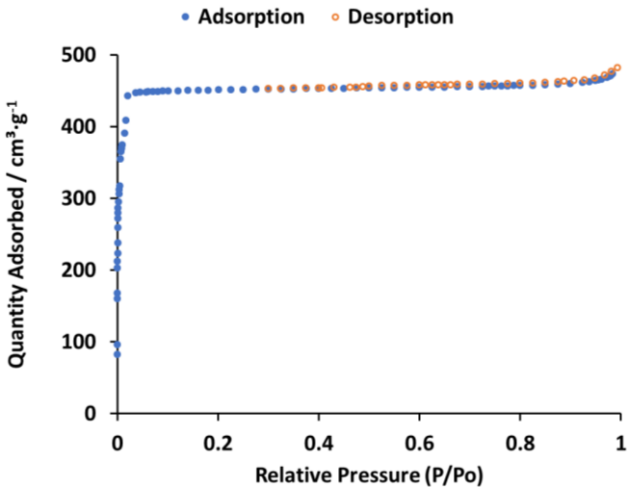

b)

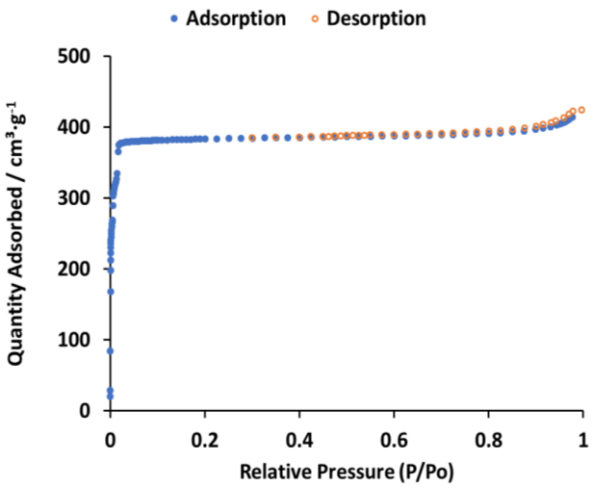

c)

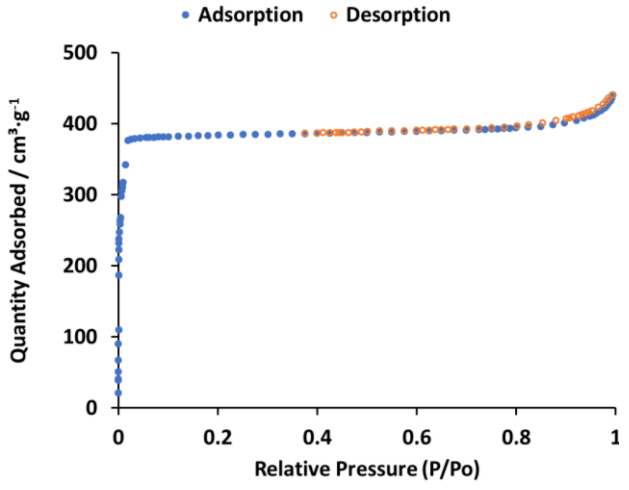

d)

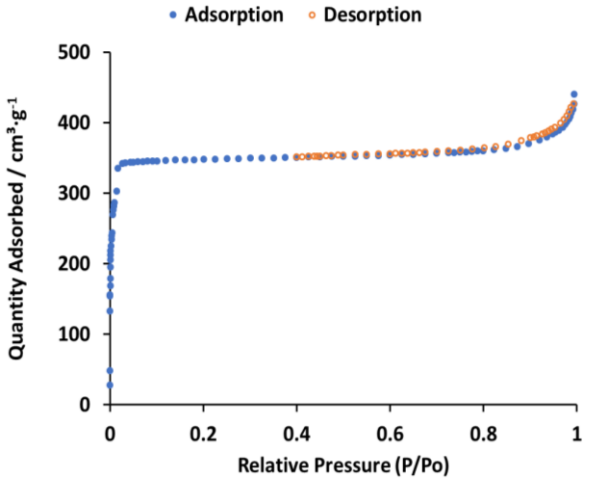

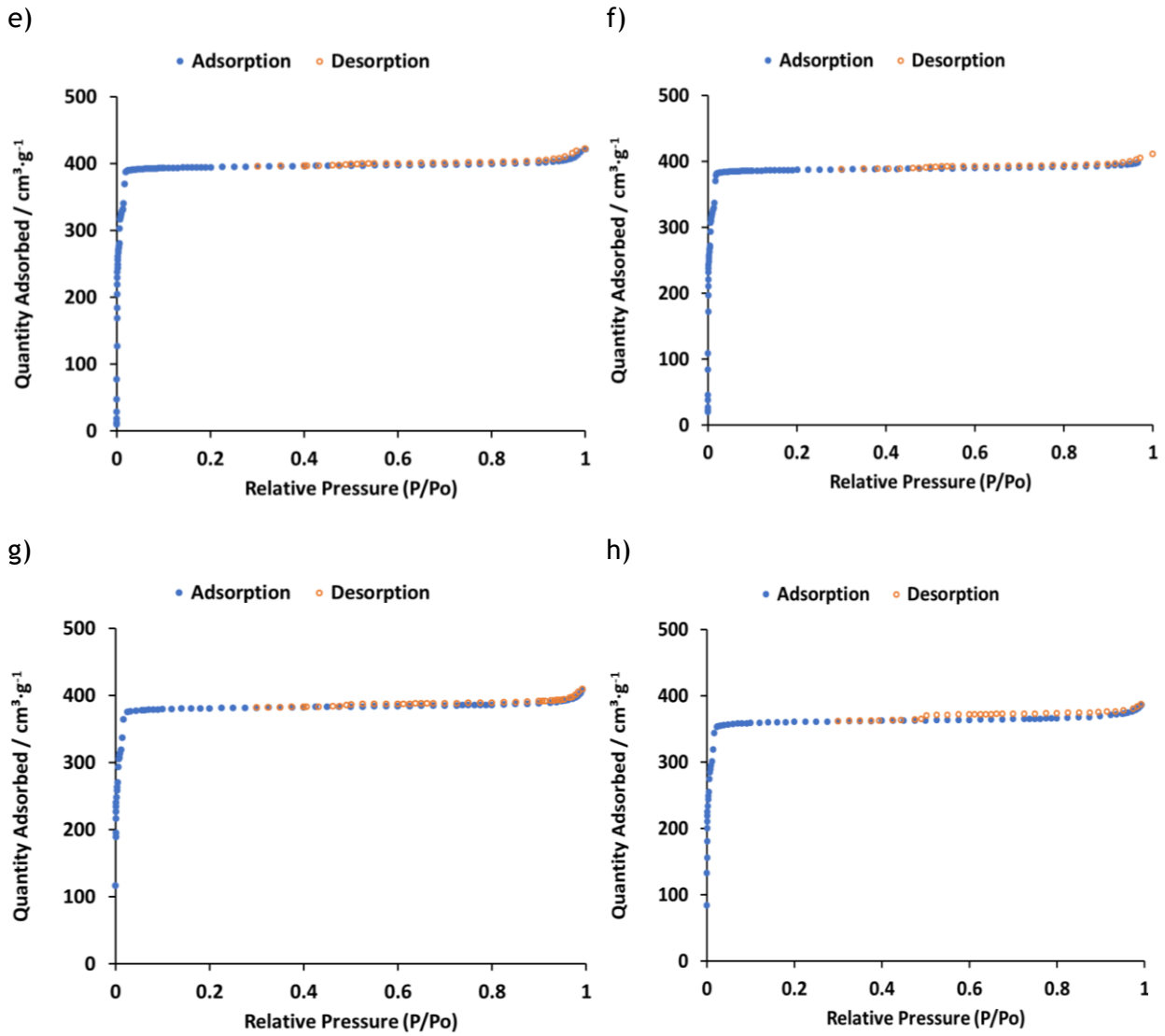

Figure D.1 - N_2 adsorption isotherms at 77 K for a) commercial ZIF-8 powder, b) ZIF-8-PA5, c) ZIF-8-PA10, d) ZIF-8-PA15, e) ZIF-8-PC5, f) ZIF-8-PC10, g) ZIF-8-MC5 and h) ZIF-8-MC10.

By observation Figure D.1 it is verified that the pristine powder and the shaped samples present a Type I isotherm characteristic of microporous materials.

For the MIL-53(Al) materials, for lower pressures an accentuated increase in the quantity of nitrogen adsorbed is verified, indicating the existence of micropores in all the materials - Figure D.2. At higher pressures (approximately $P/P_0 > 0.8$) a there is a more evident increase in the adsorbed quantity, characteristic of the capillary condensation on mesopores. This is related with "packing" of the various crystals in the powder and the network generated during shaping in the pellets, *i.e.*, the interparticle spaces [1].

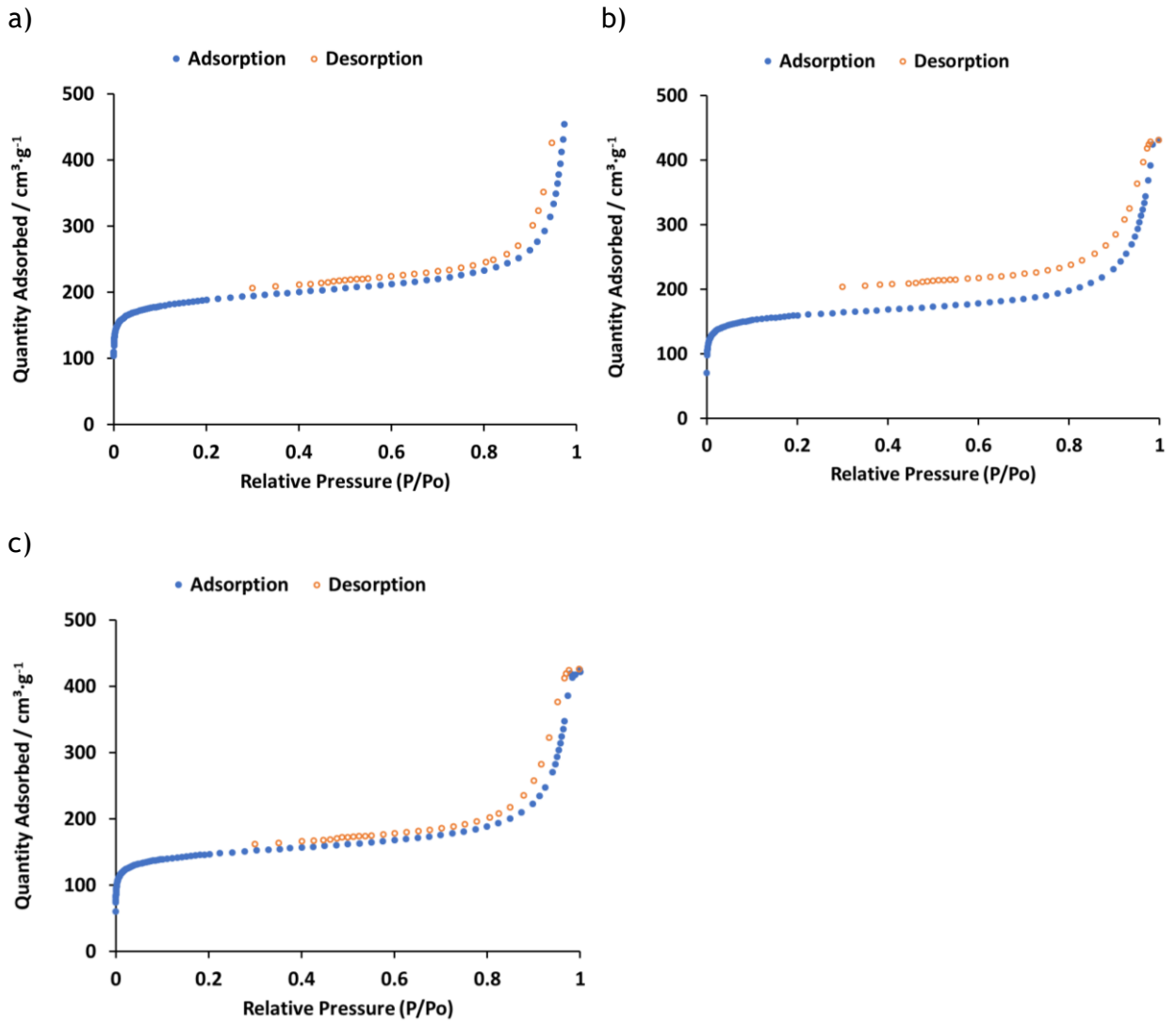

Figure D.2 - N_2 adsorption isotherms at 77 K for a) commercial MIL-53(Al) powder, b) MIL-53(Al)-PA5, c) MIL-53(Al)-PA10 and d) MIL-53(Al)-PA15.

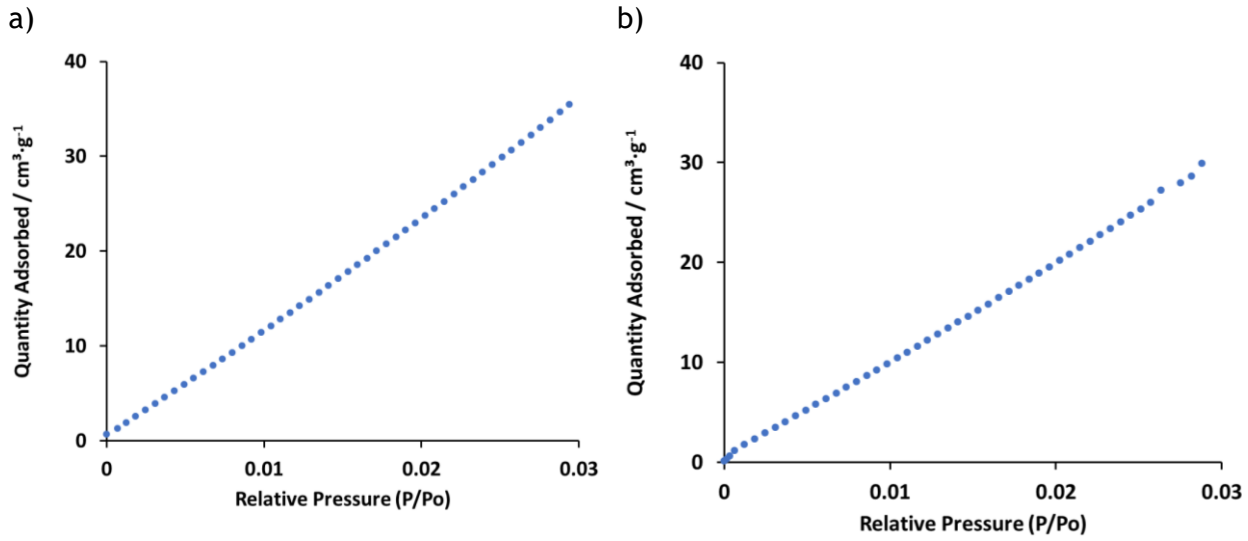

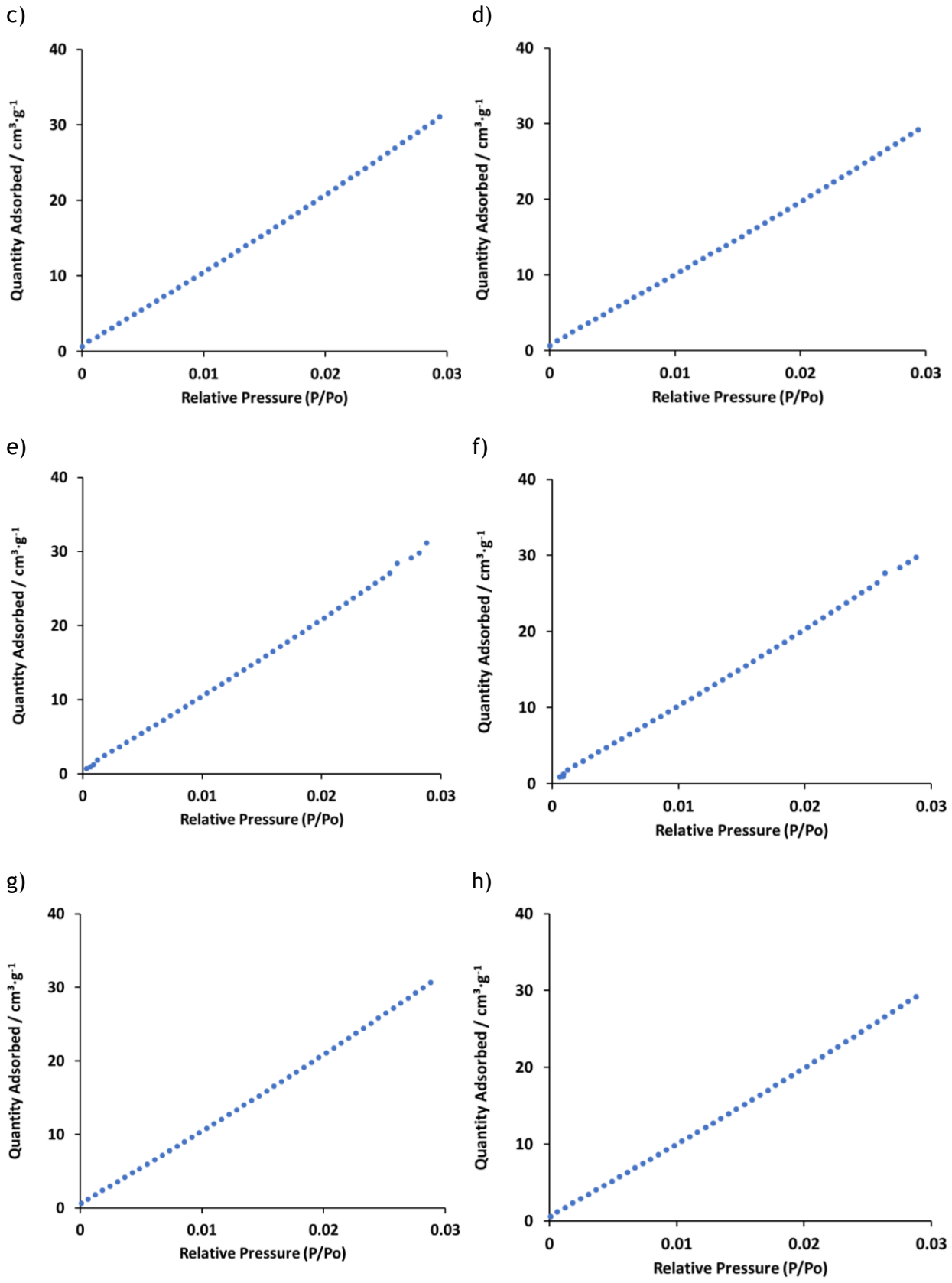

Figure D.3 - CO_2 adsorption isotherms at 273 K for a) commercial ZIF-8 powder, b) ZIF-8-PA5, c) ZIF-8-PA10, d) ZIF-8-PA15, e) ZIF-8-PC5, f) ZIF-8-PC10, g) ZIF-8-MC5 and h) ZIF-8-MC10.

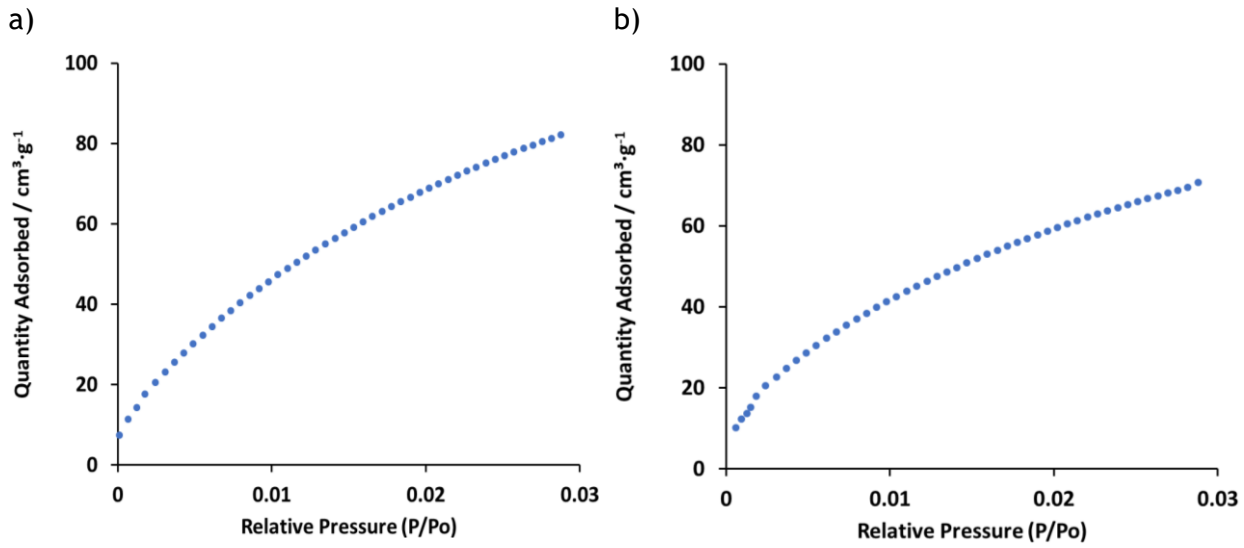

Figure D.4 - CO_2 adsorption isotherms at 273 K for a) commercial MIL-53(Al) powder, b) MIL-53(Al)-PA5, c) MIL-53(Al)-PA10, d) MIL-53(Al)-PA15.

1. Garcés, S.I., et al., *Comparative Study of the Adsorption Equilibrium of CO2 on Microporous Commercial Materials at Low Pressures*. Industrial & Engineering Chemistry Research, 2013. **52**(20): p. 6785-6793.